ACS OMEGA

http://pubs.acs.org/journal/acsodf

Article

Design of LNA Analogues Using a Combined Density Functional Theory and Molecular Dynamics Approach for RNA Therapeutics

Dikshita Dowerah, Mallikarjunachari V. N. Uppuladinne, Plaban J. Sarma, Nishant Biswakarma, Uddhavesh B. Sonavane, Rajendra R. Joshi, Suvendra K. Ray, Nima D. Namsa, and Ramesh Ch. Deka*

Cite This: *ACS Omega* 2023, 8, 22382−22405

Read Online

ACCESS | Metrics & More | Article Recommendations | Supporting Information

ABSTRACT: Antisense therapeutics treat a wide spectrum of diseases, many of which cannot be addressed with the current drug technologies. In the quest to design better antisense oligonucleotide drugs, we propose five novel LNA analogues (A1−A5) for modifying antisense oligonucleotides and establishing each with the five standard nucleic acids: adenine (A), guanine (G), cytosine (C), thymine (T), and uracil (U). Monomer nucleotides of these modifications were considered for a detailed Density Functional Theory (DFT)-based quantum chemical analysis to determine their molecular-level structural and electronic properties. A detailed MD simulation study was done on a 14-mer ASO (5′-CTTAG-CACTGGCCT-3′) containing these modifications targeting PTEN mRNA. Results from both molecular- and oligomer-level analysis clearly depicted LNA-level stability of the modifications, the ASO/RNA duplexes maintaining stable *Watson−Crick* base pairing preferring RNA-mimicking *A-form* duplexes. Notably, monomer MO isosurfaces for both purines and pyrimidines were majorly distributed on the nucleobase region in modifications A1 and A2 and in the bridging unit in modifications A3, A4, and A5, suggesting that A3/RNA, A4/RNA, and A5/RNA duplexes interact more with the RNase H and solvent environment. Accordingly, solvation of A3/RNA, A4/RNA, and A5/RNA duplexes was higher compared to that of LNA/RNA, A1/RNA, and A2/RNA duplexes. This study has resulted in a successful archetype for creating advantageous nucleic acid modifications tailored for particular needs, fulfilling a useful purpose of designing novel antisense modifications, which may overcome the drawbacks and improve the pharmacokinetics of existing LNA antisense modifications.

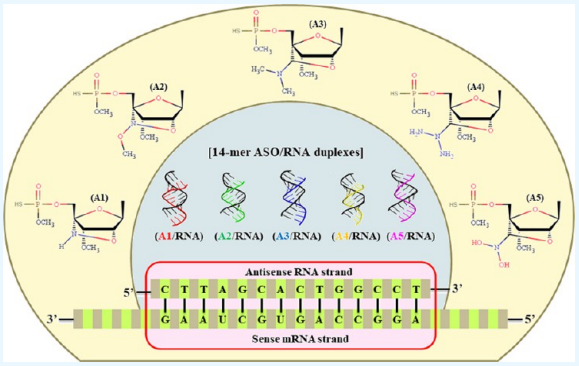

1. INTRODUCTION

Using antisense-mRNA as a medicine is a fundamentally different approach compared to treating diseases using traditional pharmaceuticals.[1−3] mRNA contains the set of instructions which direct cells in the human body to make proteins. Life depends on these proteins, as every function in the human body, both normal and disease-related, is carried out by one or many proteins in coordination. Human diseases are majorly the result of inappropriate protein production or disordered protein performance. Antisense-mRNA based drugs designed to bind sequence-specifically to their target mRNAs inhibit the production of disease-causing proteins and modulate their gene expressions. Unlike the small drug molecules and monoclonal antibodies, these synthetic antisense drugs are complementary to their sense-mRNAs, which take advantage of normal biological processes to suppress the production of disease-causing proteins and create a desired therapeutic effect.[4−6]

Antisense medications are chemically modified antisense oligonucleotides (ASOs/AONs) complementary to their target mRNAs, which bind by *Watson−Crick* base pairing, forming ASO/RNA hybrid duplexes. mRNA bound by an ASO activates the cellular endonuclease RNase H, which further cleaves the RNA strand selectively from the ASO/RNA hybrid duplexes.[7,8] However, due to the confined stability in biological media, the ASOs undergo rapid degradation even before duplexing, and thus, to protect and enhance their binding affinity and cellular uptake, the existing ASOs need to undergo chemical modifications to impart a valid antisense response. In the early stages, the phosphodiester backbones of the nucleotides were modified by replacing one of the nonbridging oxygen atoms with sulfur.[9,10] Briefly categorized under first-generation ASOs, methylphosphonates and phosphoramidates gained significant attention, yet phosphorothioates (PSs) were the most successful to induce the RNase H functions.[11−13] The first antisense drug marketed under the brand name "Vitravene" (ISIS-2922) approved by the FDA in 1998 was a

Received: December 9, 2022
Accepted: February 17, 2023
Published: June 12, 2023

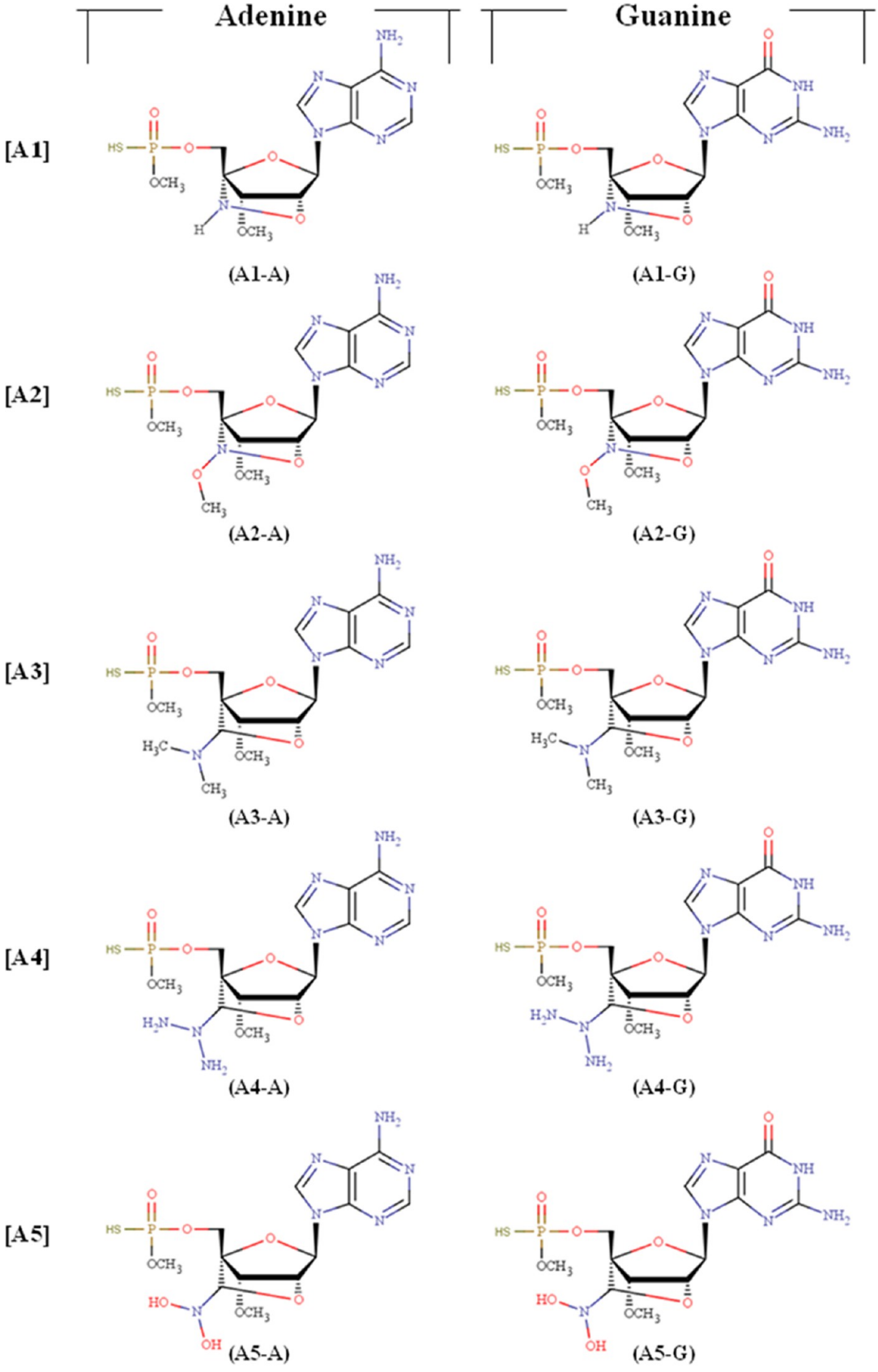

Figure 1. continued

https://doi.org/10.1021/acsomega.2c07860
ACS Omega 2023, 8, 22382−22405

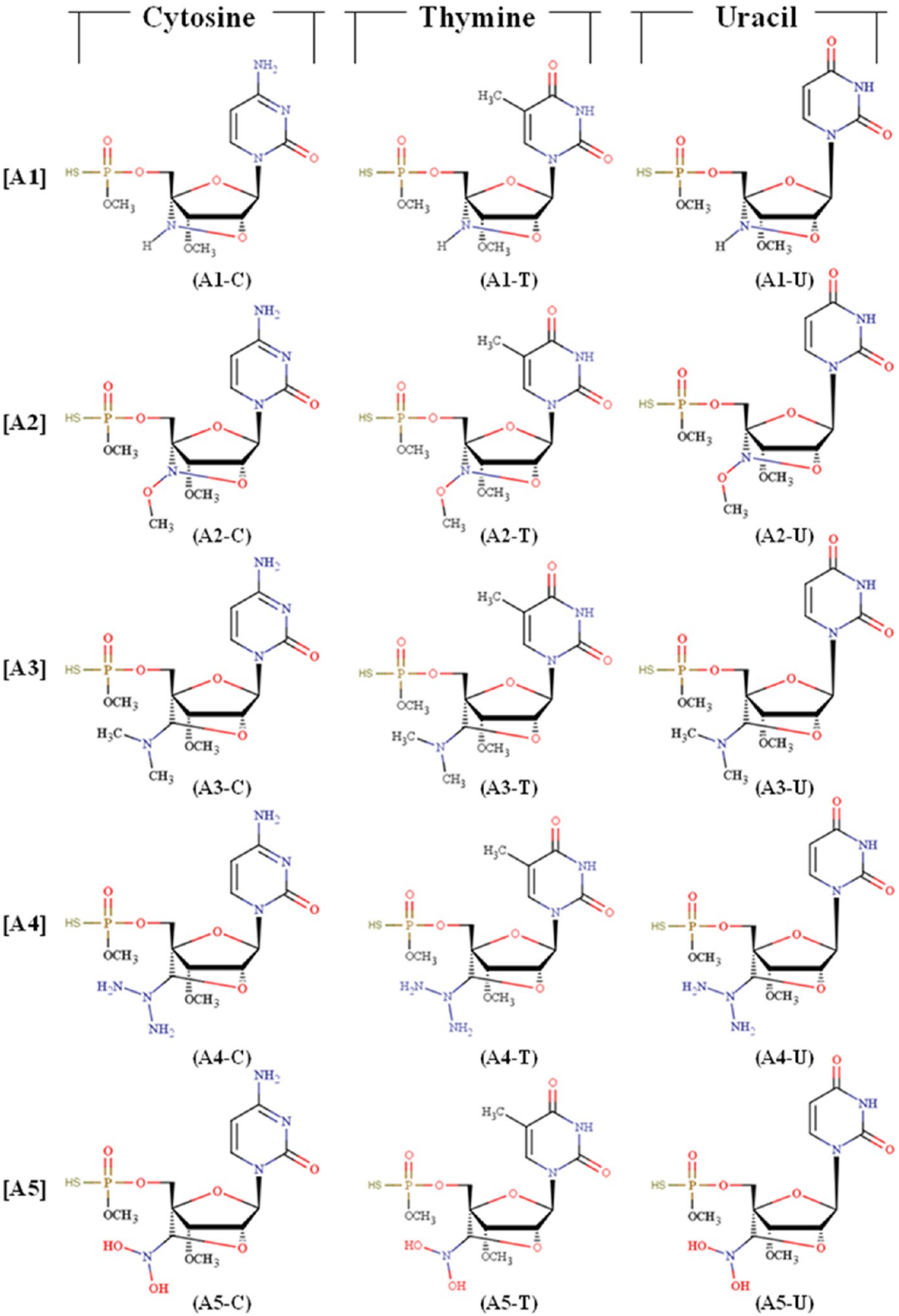

Figure 1. Schematic two-dimensional (2D) representation of the proposed LNA analogue antisense modifications A1, A2, A3, A4, and A5 each containing nucleobases adenine (A), guanine (G), cytosine (C), thymine (T), and uracil (U).

PS-oligonucleotide prescribed for the treatment of cytomegalovirus-induced retinitis.[23] However, in some cases, specificity, binding affinity to the target sequences, and cellular uptake profiles of the PSs were less satisfactory. Hence, the drawbacks of the first-generation antisense modifications were compensated by the second-generation antisense modifications, where the 2′-hydroxyl group of the furanose sugar ring was considered to further improve the pharmacokinetics of the ASOs. The 2′-O-methyl (OMe) and 2′-O-methoxyethyl (MOE) are the most well-explored second-generation

https://doi.org/10.1021/acsomega.2c07860
ACS Omega 2023, 8, 22382−22405

Table 1. Modification Details of the Proposed LNA Analogue Antisense Modifications A1, A2, A3, A4, and A5 Each Containing the Nucleobases Adenine (A), Guanine (G), Cytosine (C), Thymine (T), and Uracil (U) along with the Name Codes Used in the Present Work

Modification Type	Name Code	Nucleobases	Modification Details
A1	A1-A	A-Adenine	2′-oxygen and 4′-carbon of the sugar moiety bridged by an N-linked LNA modification + PS backbone
	A1-G	G-Guanine	
	A1-C	C-Cytosine	
	A1-T	T-Thymine	
	A1-U	U-Uracil	
A2	A2-A	A-Adenine	2′-oxygen and 4′-carbon of the sugar moiety bridged by a methoxy-N-linked LNA modification + PS backbone
	A2-G	G-Guanine	
	A2-C	C-Cytosine	
	A2-T	T-Thymine	
	A2-U	U-Uracil	
A3	A3-A	A-Adenine	2′-oxygen and 4′-carbon of the sugar moiety bridged by LNA linked to the N-dimethyl modification + PS backbone
	A3-G	G-Guanine	
	A3-C	C-Cytosine	
	A3-T	T-Thymine	
	A3-U	U-Uracil	
A4	A4-A	A-Adenine	2′-oxygen and 4′-carbon of the sugar moiety bridged by LNA linked to the N-diamine modification + PS backbone
	A4-G	G-Guanine	
	A4-C	C-Cytosine	
	A4-T	T-Thymine	
	A4-U	U-Uracil	
A5	A5-A	A-Adenine	2′-oxygen and 4′-carbon of the sugar moiety bridged by LNA linked to the N-dihydroxy modification + PS backbone
	A5-G	G-Guanine	
	A5-C	C-Cytosine	
	A5-T	T-Thymine	
	A5-U	U-Uracil	

antisense modifications reported to be less toxic with enhanced binding affinity.[14,15] To extract the utmost benefit, these sugar-based modifications were combined with the PS backbone linkage to generate chimeric ASOs, which could resolve the problem of nuclease resistance and also target binding affinity. Many such antisense molecules are available in the market as FDA-approved drugs, where both PS- and MOE-modified ASOs are being used to generate chimeric ASOs.[16−19] Several antisense drugs including *Custirsen, Fomivirsen, Mipomersen, Eteplirsen, Oblimersen, Nusinersen*, etc. have been already approved by the FDA for treating cancer, cardiovascular diseases, and various infectious and inflammatory disorders.[20−28] Third-generation antisense modifications, such as peptide nucleic acids (PNAs), locked nucleic acids (LNAs), bridged nucleic acids (BNAs), GuNA, Morpholino oligonucleotides, etc., were developed with the intention of obtaining better antisense modifications compared to those of PSs and MOEs.[29−32] LNAs are locked by a methylene bridge connecting the 2′-oxygen with the 4′-carbon of the furanose sugar ring and are reported to be the most promising third-generation antisense modification. Experimental studies carried out by medicinal chemists using LNA ASOs showed increased thermodynamic stability, nucleic acid recognition, aqueous solubility, sequence selectivity, biostability, and favorable hybridization kinetics compared to those of natural oligonucleotides.[33−35] However, these constructs could not activate the RNase H cleavage mechanism and some of their kind were undergoing rapid degradation by nucleases, being hepatotoxic.[36] The potency of these ASOs was then improved by 3−5-fold ($ED_{50} \approx 2-5$ mg/kg) without causing hepatotoxicity, which was achieved by improving the structural components of MOEs and the LNAs.[37,38] Powerful LNA analogues like the BNAs are a result of the unceasing efforts to engineer the LNA structure. BNAs are hence structural extensions of LNAs developed to overcome the drawbacks of the LNA ASOs. Following a period of research and development, the 2′,4′-BNA^{NC} analogues 2′,4′-BNA^{NC}[NH], 2′,4′-BNA^{NC}[NMe], N-Me-aminooxy BNA, and N-MeO-amino BNA have been shown to be extremely promising in overcoming the drawbacks of LNA ASOs.[39,40] BNAs are significantly more nuclease-resistant than the PSs and the LNAs in comparison. Studies on the BNA modifications conducted *in vitro* and *in vivo* revealed that when compared to MOE ASOs, optimized BNA ASOs offered greater thermal stability, enhanced *in vitro* activity, and >5-fold improved *in vivo* activity. Following this, one can attempt to design novel antisense modifications to further improve the antisense activity of existing LNA and BNA analogues.

Although there has been research on a few antisense modifications such as cyclohexyl PNA, MOE, etc., in-depth knowledge of the different antisense alterations currently in use is severely lacking and must be obtained to create superior antisense modifications.[41−47] The current study aims to design and understand the structural and functional significance of five novel LNA-based antisense modifications labeled as A1, A2, A3, A4, and A5 by establishing each with the five standard nucleic acids adenine (A), guanine (G), cytosine (C), thymine (T), and uracil (U). Previously, the modifications were designed considering the cytosine nucleobase only.[47]

https://doi.org/10.1021/acsomega.2c07860
ACS Omega 2023, 8, 22382−22405

2. MATERIALS AND METHODS

The complete methodology of the present work includes the following: First, a Density Functional Theory (DFT) based quantum chemical study was carried out to obtain the most stable conformations of the monomer nucleotides containing the proposed LNA analogue antisense modifications (A1−A5) by establishing each with the five standard nucleobases adenine (A), guanine (G), cytosine (C), thymine (T), and uracil (U) followed by derivation of quantum chemical descriptors for the same. Second, generation of forcefield parameters of all the proposed modifications corresponding to the five nucleobases A, G, C, T, and U was realized followed by a detailed Molecular Dynamics (MD) simulation study on a set of fully modified 14-mer ASO/RNA (5′-CTTAGCACTGGCCT-3′/3′-GAAUCGUGACCGGA-5′) hybrid duplex systems targeting the protein PTEN mRNA nucleic acid sequence. Schematic 2D structures of the proposed LNA analogue antisense modifications (A1−A5) each containing nucleobases adenine (A), guanine (G), cytosine (C), thymine (T), and uracil (U) are given in Figure 1, and the modification details are listed in Table 1.

2.1. Density Functional Theory (DFT) Calculations. Starting structures of the modifications were built on the LNA monomer nucleotide structures using the Discovery Studio and Gauss View program packages.[48,49] DFT-based quantum chemical calculations were carried out to obtain optimized structures and ground-state energies of all the monomer nucleotides using the Gaussian09 software package.[49] Full geometry optimization along with frequency calculations was done employing the meta-GGA, hybrid, unrestricted M06-2X functional alongside triple-ζ split valence, and diffused basis set 6-311G(d,p) for all atoms, without imposing any symmetry constraints.[50−53] Using the conductor-like polarizable continuum solvation model (CPCM), water (with a dielectric constant of 78.39) was added as the solvent implicitly.[54] Natural bond orbital (NBO) calculations were performed on the optimized structures at the same level of theory to generate wavefunction files. Molecular orbital composition analysis was carried out to find out the composition of the highest occupied molecular orbital−least unoccupied molecular orbital (HOMO−LUMO) isosurfaces using the opensource Multiwfn software program.[55]

2.1.1. Global Reactivity Descriptors. *Koopmans'* theorem states that IP and EA values are the negative of energy eigenvalues, with IP = $-E_{HOMO}$ and EA = $-E_{LUMO}$. These fundamental equations are applied to the analysis of a set of global parameters that characterize the structural transitions between different ground states. Global reactivity descriptors global hardness (η), global softness (S), chemical potential (μ), and electrophilicity (ω) all were evaluated using the following equations as described below.[56−58]

$$\text{global hardness } (\eta) = (\text{IP} - \text{EA})/2$$

$$\text{global softness } (S) = 1/2\eta$$

$$\text{chemical potential } (\mu) = -(\text{IP} + \text{EA})/2$$

$$\text{electrophilicity } (\omega) = \mu^2/2\eta$$

2.2. Molecular Dynamics (MD) Simulations. *2.2.1. System Building and Forcefield Parameters.* Forcefield parameters were developed for the proposed antisense modifications (A1−A5) corresponding to the five nucleobases using the parameterization protocol given in the literature.[59,60] Partial atomic charges were derived at the M06-2X/-311G** level of theory using the Gaussian09 program package.[49] RESP fitting was done using the ANTECHAMBER module of AMBER18.[61] After parameterization, a set of 14-mer ASO/RNA hybrid duplex systems composed of the fully modified 14-mer (5′-CTTAGCACTGGCCT-3′) ASO strand containing the proposed modifications (A1−A5) and 14-mer (3′-GAAUCGUGACCGGA-5′) RNA strand as the target complementary sequence were built. Since the modifications are LNA-based, a regular LNA/RNA hybrid has been considered the control system for comparison. The systems were charge-neutralized adding Na^+/Cl^- as counter ions and solvated explicitly with a TIP3P water box.[62] The entire duplex building process was carried out using the leap module of AMBER implementing the standard forcefield parameters "RNA.OL3" for RNA nucleobases and the in-house generated forcefield parameters for the proposed antisense modifications.[63,64]

2.2.2. Simulation Protocol and Trajectory Analysis. Simulations were carried out using the all-atom classical MD simulation framework of AMBER18. The systems were energy-minimized using the steepest descent method for 5000 steps, followed by 5000 steps conjugate gradient method. Energy minimization was done using constraints of 100 kcal/mol initially and then gradually reducing the constraints on all the solute atoms. The systems were then heated slowly from 0 to 300 K in a canonical ensemble using constraints of 100 kcal/mol on all the solute atoms. After heating, the systems underwent equilibration in an isothermal isobaric (NPT) ensemble in a similar way using constraints of 100 kcal/mol initially and gradually reducing the constraints on all the solute atoms. Simulations were performed under periodic boundary conditions using the particle mesh Ewald technique to account for the long-range electrostatics.[65] MD integration was carried out using 2.0 fs time step, employing the SHAKE algorithm on all the bonds involving hydrogen atoms.[66] For nonbonding interactions, a cutoff distance of 10 Å was used. The systems were then allowed to simulate under production run conditions for 100 ns and the trajectories were used for analysis. The CPPTRAJ module of AmberTools was used for trajectory analysis.[67] Solvent-accessible surface area (SASA) was calculated for all the duplexes using the VMD program.[68] The MM-GBSA module of AMBER was used for calculating the free energy of the duplexes.[69,70]

3. RESULTS AND DISCUSSION

3.1. DFT Results. *3.1.1. Structure and Energetics of the LNA Analogue Monomer Nucleotides.* LNAs are RNA derivatives in which a methylene bridge locks the 2′-oxygen with the 4′-carbon of the ribose sugar ring. The bridge causes a *C3′-endo* sugar puckering geometry, which decreases the ribose's conformational flexibility and increases the local organization of the phosphate backbone. LNAs have stronger binding properties compared to those of MOE antisense modifications but at the same time higher toxicity compared to the same.[36] To develop highly active ASO/mRNA therapeutic antisense candidates, it is inevitable to enhance the potency and reduce the probable toxicity of the existing LNA ASOs. In the present study, we propose five novel LNA analogue antisense modifications A1, A2, A3, A4, and A5 by establishing each with all the five standard nucleobases adenine (A), guanine (G), cytosine (C), thymine (T), and uracil (U). The

https://doi.org/10.1021/acsomega.2c07860
ACS Omega 2023, 8, 22382−22405

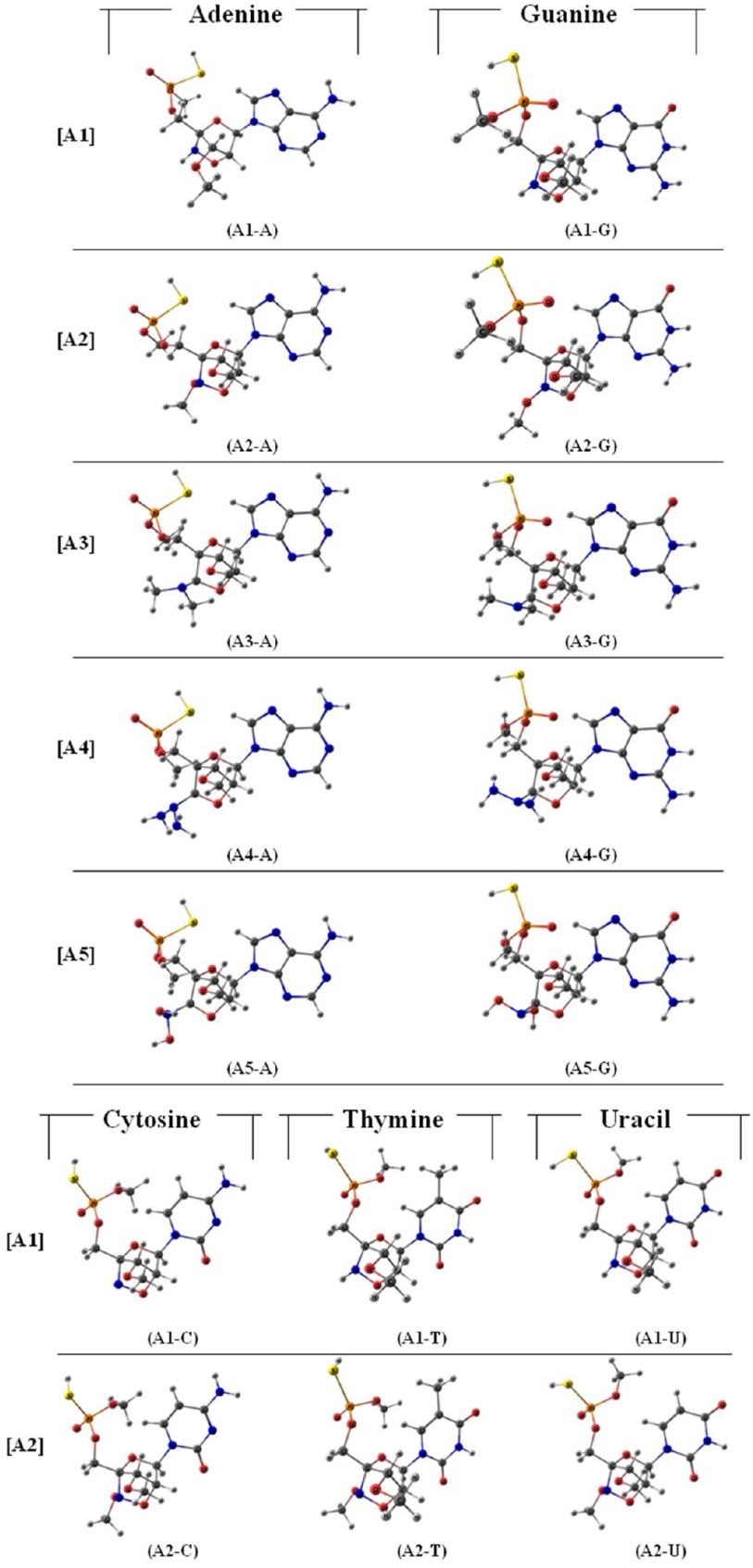

Figure 2. continued

https://doi.org/10.1021/acsomega.2c07860
ACS Omega 2023, 8, 22382−22405

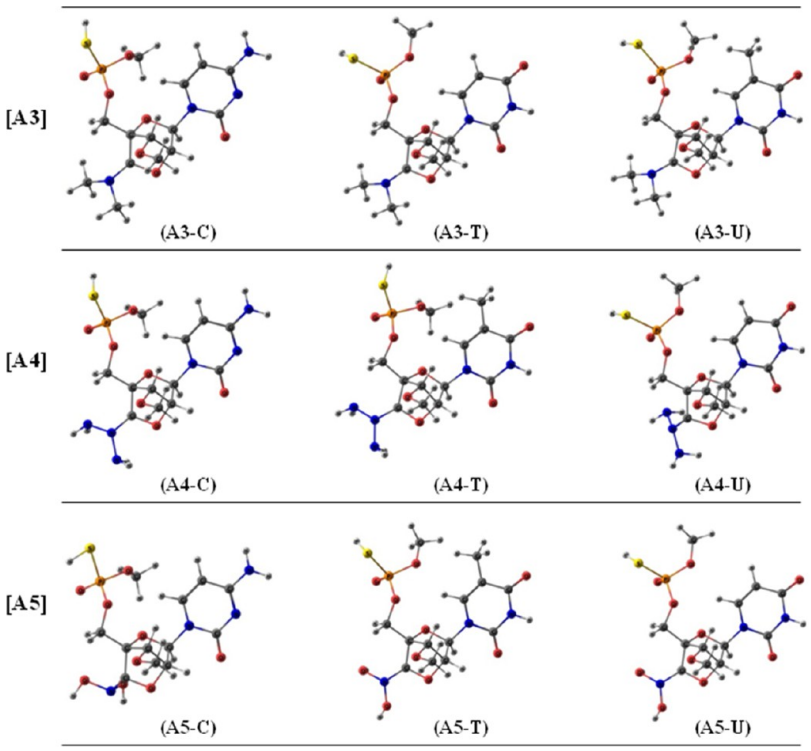

Figure 2. Optimized structures of the proposed LNA analogue antisense modifications A1, A2, A3, A4, and A5 with their respective nucleobases adenine (A), guanine (G), cytosine (C), thymine (T), and uracil (U) calculated at the M06-2X/6-311G(d,p) level of theory.

modifications are LNA-based and have been designed considering the structural motifs of standard antisense modifications from the literature. In all the modifications, the 2′-oxygen and 4′-carbon of the ribose sugar ring are linked to each other by five different conformationally constrained functional groups, designed by infusing different oxy or nitro groups into the parent LNA structure. Keeping in mind the importance of nitrogen chemistry in natural nucleic acids, in modifications A1 and A2, the methylene bridge carbon of the LNA is replaced with nitrogen. In A2, an extra methoxy group is added to the bridged nitrogen. In A3, A4, and A5, N-dimethyl, N-diamine, and N-dihydroxy groups were added to the LNA carbon of the methylene bridge, respectively. Methoxy motifs have been well established in 2′-oxygen sugar modifications, and their incorporation has already been proven to show better pharmacokinetic properties.[19] Metabolic stability and cellular uptake of modified ASOs are immensely improved by phosphorothioate (PS) modifications in coordination with sugar-based modifications. PS substitutions are known to immensely induce RNase H activity, serum stability, and cellular uptake of modified ASOs, and hence, all the modifications were further impregnated involving the PS backbone linkage. Thus, the proposed modifications are designed in a way such that they share the structural components of LNA, BNA, MOE, and PSs along with other electronegative groups attached to the methylene bridge carbon of LNA. BNAs are structural extensions of LNAs developed to improve the drawbacks of existing LNA ASOs. The basic idea behind functionalizing the LNAs is to reduce the hepatotoxicity and enhance the overall pharmacokinetic properties of the LNA ASOs without disturbing the strong binding nature of LNAs.

LNA nucleotides are linked by similar phosphodiester linkages resembling the natural nucleic acids found in DNA and RNA with respect to adequate aqueous solubility and the *Watson−Crick* mode of binding.[71] These similarities of LNA nucleotides compared to the DNA and RNA nucleotides attribute to the use of standard reagents and automated synthesizers, facilitating their handling and simplifying the experiments to synthesize them using conventional phosphoramidite chemistry. Also, mixing of DNA and RNA bases allows the affinity for complementary sequences or the susceptibility to RNase H to be optimized for individual applications, which further allows LNA-containing nucleotides to be interspersed among DNAs and RNAs.[72] However, to fine-tune the LNAs, it is highly needed to have adequate information on the structure and electronic properties of the existing as well as novel antisense proposals. Now, a molecular structure comprises the distinctive elements that give rise to its physical, chemical, and biological capabilities, and a detailed quantum chemical study of the molecular geometries can aid in identifying the structure−activity link of related compounds. Herein, we report an elaborate study on the proposed antisense modifications at both the monomer and oligomer levels. All the monomer nucleotides were subjected to a DFT-based full geometry optimization followed by single-point energy calculations on the optimized structures to evaluate their various structural and electronic properties at the monomer level. Optimized structures of the proposed LNA analogue antisense modifications (A1−A5) each containing nucleobases A, G, C, T, and U calculated at the M06-2X/6-311G(d,p) level of theory are given in Figure 2. The calculated IR spectra of the monomer nucleotides are also given in Figure S1 (SI).

To inhibit the production of disease-causing proteins, the synthetic ASOs should be able to bind to their target mRNAs, inhibit the protein synthesis, and modulate their gene expressions. The methylene bridge of the ribose in LNAs constricts sugar puckering into the desired *C3′-endo* con-

https://doi.org/10.1021/acsomega.2c07860
ACS Omega 2023, 8, 22382−22405

Table 2. Chi (χ) Torsion Angle, Electronic Energy, Dipole Moment, E_{HOMO}, E_{LUMO}, and ΔE_{gap} of the Proposed LNA Analogue Antisense Modifications A1, A2, A3, A4, and A5 with Their Respective Nucleobases Adenine (A), Guanine (G), Cytosine (C), Thymine (T), and Uracil (U) Calculated at the M06-2X/6-311G(d,p) Level of Theory

Name Code	Chi (χ)	Electronic nergy (Hartree)	Dipole Moment (D)	E_{HOMO} (eV)	E_{LUMO} (eV)	ΔE_{gap} (eV)
A1-A	−178.7	−1986.774755	5.90	−7.674	0.036	7.710
A1-G	−166.5	−2062.022488	9.71	−7.343	0.553	7.897
A1-C	−165.1	−1914.404476	9.86	−7.999	−0.134	7.865
A1-T	−164.9	−1973.596417	6.51	−7.996	−0.168	7.828
A1-U	−166.6	−1934.286304	6.21	−8.267	−0.259	8.008
A2-A	−176.8	−2101.239983	4.72	−7.682	0.028	7.710
A2-G	−169.7	−2176.485949	10.78	−7.352	0.541	7.893
A2-C	−165.8	−2028.871153	8.73	−8.034	−0.147	7.887
A2-T	−162.1	−2088.063050	2.57	−8.048	−0.226	7.821
A2-U	−167.5	−2048.751847	4.46	−8.290	−0.275	8.016
A3-A	−173.0	−2104.069445	4.86	−5.766	−0.109	5.658
A3-G	−167.8	−2179.314657	10.32	−6.005	−0.102	5.903
A3-C	−164.7	−2031.698037	7.35	−5.844	−0.245	5.599
A3-T	−163.9	−2090.889118	5.81	−5.879	−0.277	5.601
A3-U	−164.5	−2051.579474	6.64	−5.846	−0.297	5.549
A4-A	−173.4	−2136.108387	9.14	−6.617	−0.475	6.142
A4-G	−167.3	−2211.355947	9.75	−6.402	−0.194	6.208
A4-C	−164.5	−2063.741769	6.36	−6.108	−0.439	5.669
A4-T	−161.3	−2122.933761	2.88	−6.144	−0.474	5.670
A4-U	−166.9	−2083.619682	3.50	−6.253	−0.283	5.969
A5-A	−172.9	−2175.811314	8.48	−7.241	−0.788	6.453
A5-G	−165.5	−2251.060222	13.01	−7.000	−0.656	6.344
A5-C	−163.9	−2103.442453	5.87	−7.019	−0.690	6.329
A5-T	−164.0	−2162.632384	4.26	−6.848	−0.993	5.855
A5-U	−166.4	−2123.322541	4.94	−6.859	−0.988	5.871

formation, an important consideration for antisense therapeutic applications.[73] Also, the LNAs in complex with RNAs induce flanking RNA bases to adopt an *N-type* conformation, which favors *C3′-endo* sugar puckering and activates RNase H cleavage of the bound RNAs. From the optimized structures, it was observed that the sugar puckering criterion is fulfilled, which showed no disturbance in the *N-type* conformation due to the infusion of the proposed modifications. Also, to bind sequence-specifically to their target RNAs, the modified LNA monomer nucleotides should exist in an *anti*-conformation, a property of the *A-form* helix generally observed in RNAs. The chi (χ) torsion angle specifies the relative sugar/base orientation in standard nucleic acids. Chi (χ) values of all the modified nucleotides are listed in Table 2. In general, "χ" falls in the range of +90 to +180°/−90 to −180° (or 180−270°) corresponding to the *anti*-conformation in *A-form* nucleic acid duplexes.[74] From Table 2, χ values of the modified LNA nucleotides suggest their relative sugar/base orientations to be in the *anti*-conformation, which can increase the strength of base pairing and base stacking interactions preferring the RNA-mimicking *A-form* helix during duplex formation.

3.1.2. Molecular Orbital Analysis of the LNA Analogue Monomer Nucleotides. The frontier molecular orbitals HOMO−LUMO are important quantum chemistry metrics, which can reveal minute details about the accessible binding sites within the LNA analogue monomer nucleotides for interactions with the host molecules. The HOMO energy (E_{HOMO}), LUMO energy (E_{LUMO}), and the differences in their HOMO−LUMO energy gap (ΔE_{gap}) are therefore important indicators when taking into account the chemical reactivity and stability, which can provide detailed information on the bonding nature of the monomer nucleotides. The calculated electronic energies, dipole moment, and energies values of E_{HOMO}, E_{LUMO}, and ΔE_{gap} of the LNA analogue monomer nucleotides estimated at the M06-2X/6-311G(d,p) level of theory are listed in Table 2 and plotted in Figure 3. A detailed study as such on the HOMO−LUMO energies would provide an in-depth scope to relate variations in the molecular properties of the proposed antisense modifications. In the case of the purine nucleobases, modifications A1 and A2 have low-lying E_{HOMO} and high-lying E_{LUMO} and modifications A3, A4, and A5 have high-lying E_{HOMO} and low-lying E_{LUMO} for both the nucleobases adenine and guanine. In the case of the pyrimidine nucleobases, again, the modifications A1 and A2 have low-lying E_{HOMO} and high-lying E_{LUMO} and modifications A3, A4, and A5 have high-lying E_{HOMO} and low-lying E_{LUMO} for all the three nucleobases cytosine, thymine, and uracil. Now, E_{HOMO} of a molecule determines the electron donating ability and E_{LUMO} determines the ability of the molecule to accept electrons. The higher the E_{HOMO}, the better the electron donating capacity, and the lower the E_{LUMO}, the better the electron accepting capacity. Thus, for both the purine and pyrimidine nucleobases, there is the possibility of modifications A3, A4, and A5 to be better electron donors as well as better electron acceptors compared to modifications A1 and A2. Accordingly, the ΔE_{gap} values for modifications A3, A4, and A5 were lower compared to those of modifications A1 and A2 for both the purines and pyrimidines.

Molecular orbital compositions of the proposed LNA analogue monomer nucleotides containing nucleobases A, G, C, T, and U were studied by observing the orientation and composition of their HOMO−LUMO isosurfaces, estimated at the M06-2X/6-311G(d,p) level of theory, presented in Figure

https://doi.org/10.1021/acsomega.2c07860
ACS Omega 2023, 8, 22382−22405

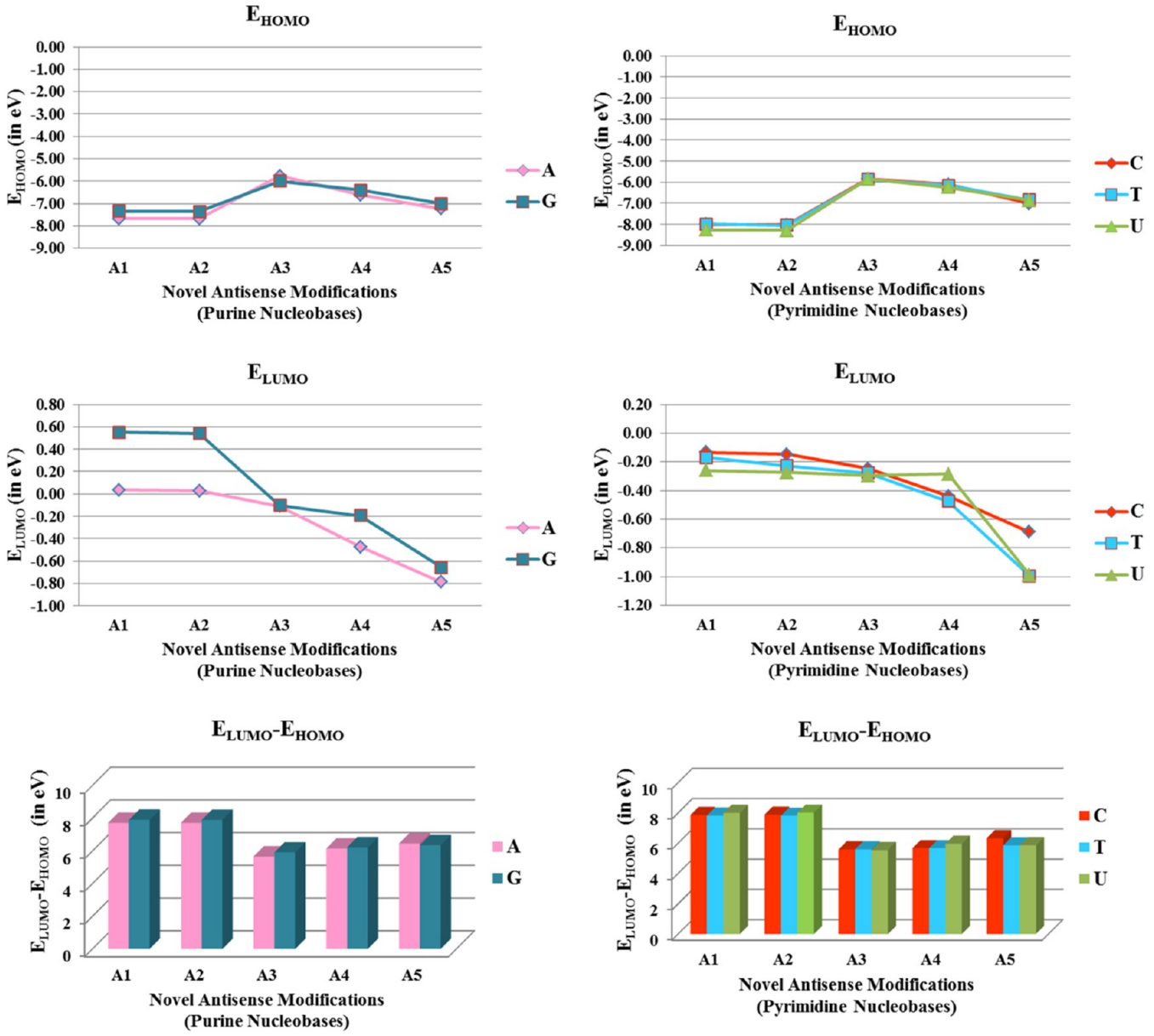

Figure 3. E_{HOMO}, E_{LUMO}, and ΔE_{gap} of the proposed LNA analogue antisense modifications A1, A2, A3, A4, and A5 with their respective nucleobases adenine (A), guanine (G), cytosine (C), thymine (T), and uracil (U) calculated at the M06-2X/6-311G(d,p) level of theory.

4a−e, respectively. A detailed study on the molecular orbital compositions would cover an intensive scope to relate the bonding nature of the different antisense modifications bearing similar parent molecular structures. HOMO−LUMO isosurfaces of modifications A1 and A2 for both A and G are majorly distributed on the nucleobase region. Being embedded within the nucleobase might decrease their interactions with the RNase H and solvent environment. However, in the modifications A3, A4, and A5, both the HOMO and LUMO isosurfaces are well distributed in the modified bridging LNA unit, which will be comparatively more available for interactions with the RNase H and solvent environment. The % contributions of each orbital to the HOMO−LUMO were also calculated and are listed in Table S1 (SI). Analyzing the detailed orbital composition of the HOMO and LUMO, it was observed that in the modifications A1-A and A2-A, the major contributors of the HOMO and LUMO are the 2p orbitals of N(18) and C(13) atoms, respectively. In the modifications A3-A, A4-A, and A5-A, the major contributors of both the HOMO and LUMO are the 2p orbital of the C(42) atom. In the modifications A1-G and A2-G, the major contributors of the HOMO and LUMO are the 2p orbitals of C(15) and C(16) atoms, respectively. In the modifications A3-G, A4-G, and A5-G, the major contributors of both the HOMO and LUMO are the 2p orbital of the C(43) atom.

In the modifications A3, A4, and A5, both the HOMO and LUMO isosurfaces are well distributed in the modified bridging LNA-containing region. In the modifications A1-C and A2-C, the major contributors of the HOMO and LUMO are the 2p orbitals of C(3) and C(2) atoms, respectively. In the modifications A3-C, A4-C, and A5-C, the major contributors of both the HOMO and LUMO are the 2p orbital of the C(39) atom. In the modifications A1-T and A2-T, the major contributors of the HOMO and LUMO are the 2p orbitals of C(10) and C(4) atoms, respectively. In the modifications A3-T, A4-T, and A5-T, the major contributors of both the HOMO

https://doi.org/10.1021/acsomega.2c07860
ACS Omega 2023, 8, 22382−22405

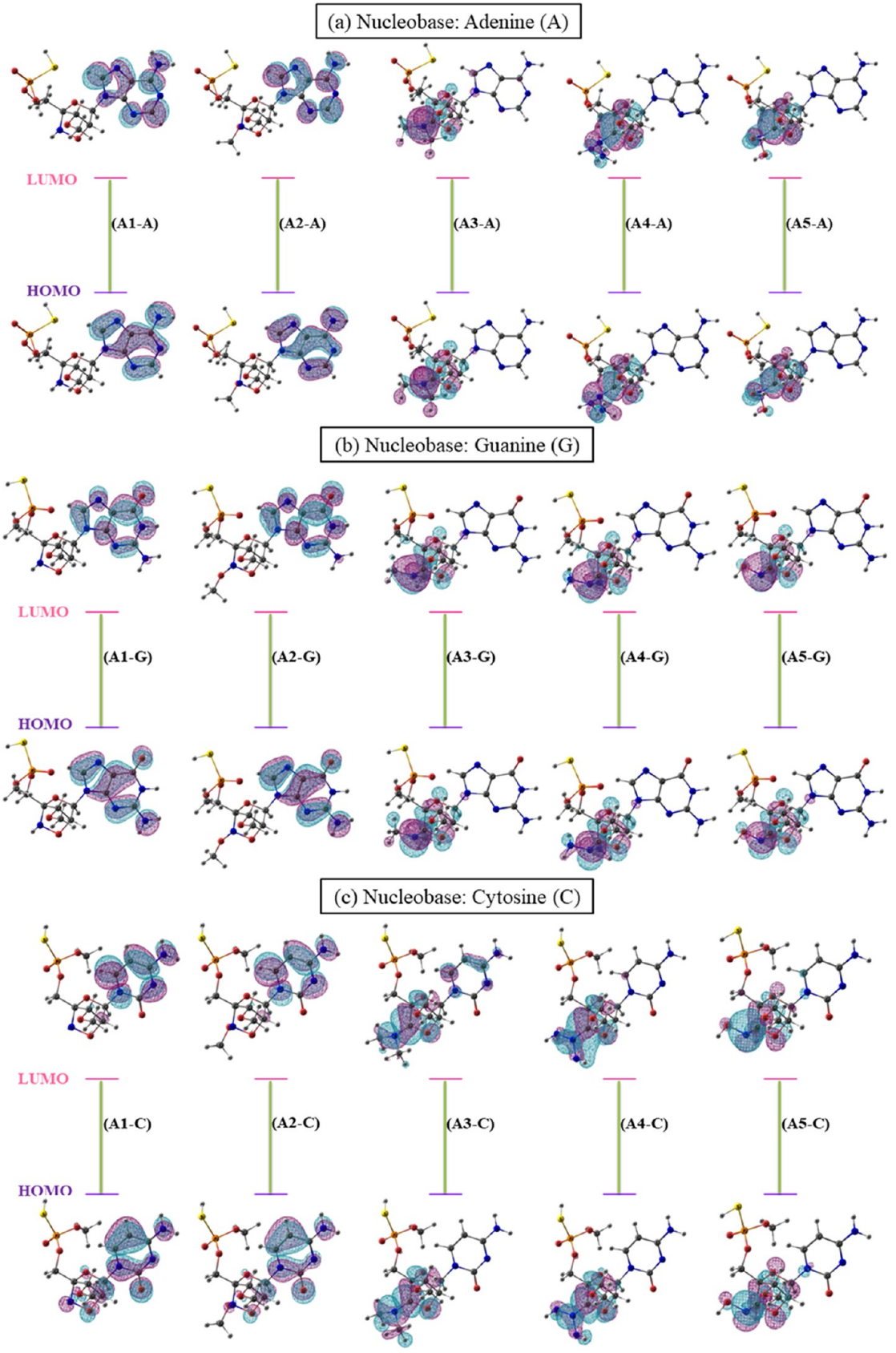

Figure 4. continued

https://doi.org/10.1021/acsomega.2c07860
ACS Omega 2023, 8, 22382−22405

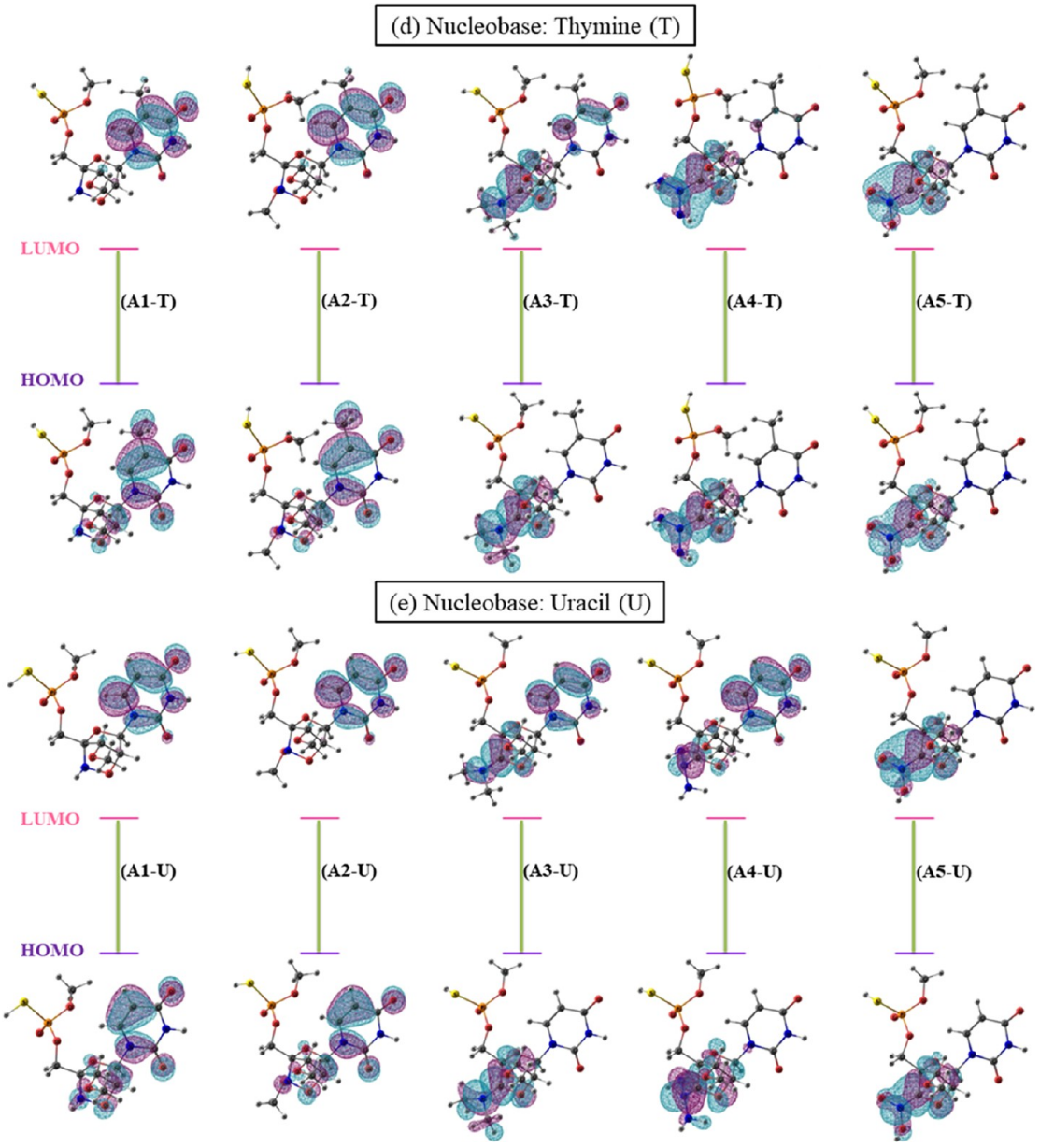

Figure 4. HOMO and LUMO isosurfaces of monomer nucleotides of the proposed LNA analogue antisense modifications (A1−A5) each containing nucleobase (a) adenine (A), (b) guanine (G), (c) cytosine (C), (d) thymine (T), and (e) uracil (U) calculated at the M06-2X/6-311G(d,p) level of theory.

and LUMO are the 2p orbital of the C(42) atom. In the modifications A1-U and A2-U, the major contributors of the HOMO and LUMO are the 2p orbitals of C(10) and C(4) atoms, respectively. In the modifications A3-U and A5-U, the major contributors of both the HOMO and LUMO are the 2p orbital of the C(38) atom. In the modification A4-U, the major contributors of the HOMO and LUMO are the 2p orbital of the C(39) atom and C(4) respectively. Overall, the modifications A1 and A2 have higher ΔE_{gap} for both purine and pyrimidine nucleobases and the modifications A3, A4, and A5 have lower ΔE_{gap} for the same.

3.1.3. Global Reactivity Descriptors of the LNA Analogue Monomer Nucleotides. A brief analysis on the HOMO−LUMO energies is of ample importance considering the bonding nature of molecules. However, alongside that, a detailed study on the global reactivity descriptors derived from the HOMO−LUMO energies can provide an in-depth scope to predict the drug-like nature of the proposed antisense alterations. According to these descriptors, the extent of chemical reactivity and stability of a molecule varies with changing structural configuration of the molecules. Such a type of study has been used by several research groups for small drug molecules and their derivatives bearing similar molecular structures including a few modified nucleobases as well. In the present work, we have used a similar strategy to study the quantum chemical reactivity descriptors of monomer nucleotides of the proposed LNA analogue antisense modifications. The calculated global reactivity descriptors global hardness (η), global softness (S), chemical potential (μ), and electrophilicity (ω) of the monomer nucleotides of the proposed LNA analogue antisense modifications (A1−A5) with their respective nucleobases A, G, C, T, and U estimated at the M06-2X/6-311G(d,p) level of theory are shown Figure S2 (SI) and listed in Table S2 (SI).

https://doi.org/10.1021/acsomega.2c07860
ACS Omega 2023, 8, 22382−22405

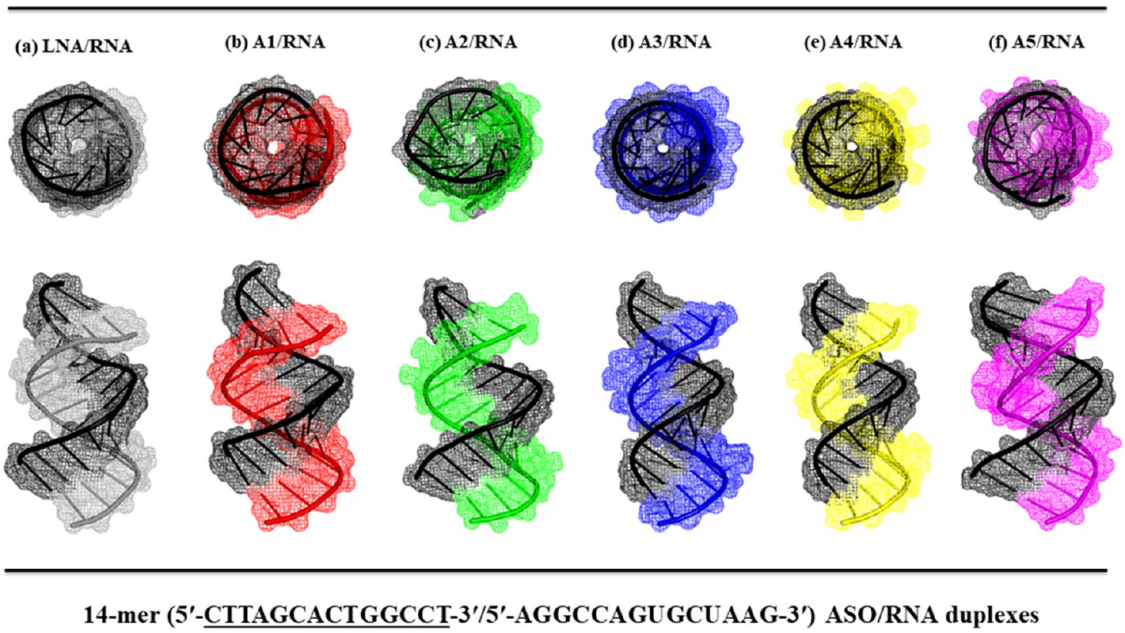

Figure 5. Structures of 14-mer ASO/RNA duplexes, (a) LNA/RNA, (b) A1/RNA, (c) A2/RNA, (d) A3/RNA, (e) A4/RNA, and (f) A5/RNA, considered for the MD simulation study.

Global hardness (η) and global softness (S) give us a qualitative demonstration of how polarizable a molecule is and give us an indication of resistance to deformation. Hard molecules do not have easily excitable outer electrons and are less polarizable. It is associated with low-lying E_{HOMO} and high-lying E_{LUMO}. Qualitatively, global softness (S) is the reciprocal of hardness. Associated with high-lying E_{HOMO} and low-lying E_{LUMO}, soft molecules have easily accessible outer electrons and are more polarizable compared to the hard molecules. Thus, hard molecules will have a higher ΔE_{gap} compared to that of soft molecules. In general, a molecule with a high ΔE_{gap} is considered chemically more stable, while that with a small ΔE_{Gap} is considered chemically more reactive. Results of ΔE_{Gap}, global hardness (η), and global softness (S) revealed that modifications A3, A4, and A5 will be more active in electron receiving and elimination processes or softer in chemical reactions compared to modifications A1 and A2 irrespective of the type of nucleobase, be it the purines or the pyrimidines.

Chemical potential (μ) and electrophilicity (ω) are two further associated metrics that can be utilized to estimate the monomer nucleotides' relative reactivity. The chemical potential (μ) mentioned here is the electronic chemical potential that measures an infinitesimal change in energy upon addition of an electronic charge. Results from chemical potential (μ) values suggest that modifications A1, A2, and A5 have more negative chemical potential values and modifications A3 and A4 have less negative chemical potential values for the purines, and on the other hand, modifications A1 and A2 have more negative chemical potential values and modifications A3, A4, and A5 have less negative chemical potential values for the pyrimidines. Aa an indicator of a system's responsiveness to nucleophiles and electrophiles, electrophilicity (ω) is connected to the stabilization of energy when a system becomes saturated with electrons from the outside environment. Lower values of ω indicate the presence of a good nucleophilic character, while higher values of ω indicate the presence of a good electrophilic character. Electrophilicity values suggest that modifications A3 and A4 are less electrophilic, while modifications A1, A2, and A5 are more electrophilic irrespective of the type of nucleobase, be it the purines or the pyrimidines. This is an implication of A3 and A4 having high-lying E_{HOMO}, which will accept electrons less easily rather that donating more easily, hence being less electrophilic, compared to A1, A2, and A5 having low-lying E_{HOMO}, which will donate electrons less easily rather than accepting more easily, hence being more electrophilic. Overall, modifications A3 and A4 have less negative chemical potential and are less electrophilic compared to A1, A2, and A5 for both the purine and pyrimidine nucleobases.

3.2. MD Simulation Results. *3.2.1. Dynamics of the Proposed LNA Analogue ASO/RNA Oligomer Duplexes.* Experimenting design possibilities of novel LNA analogues has resulted in numerous LNA antisense alterations of being investigated for a variety of potential biological activities. Being incorporated into the oligomeric nucleic acid duplexes, the proposed modifications will reorganize the structural and dynamic properties of the modified ASO/RNA duplexes as a whole. Also, it is unwise to design the analogues without first confirming their ability to strongly duplex with the targets, particularly a natural source as mRNA. Thus, a detailed MD simulation study was carried on fully modified 14-mer (5′-CTTAGCACTGGCCT-3′/3′-GAAUCGUGACCGGA-5′) ASO/RNA hybrids containing the modifications A1−A5, over 100 ns simulation trajectory data. A sampling time of 100 ns of the simulation was considered noting the smaller size of the duplexes. Previous experimental studies targeting the protein PTEN using LNA and MOE modifications in mice have resulted in an increased potency of second-generation ASOs by reducing the length of the ASOs from 20-mer to 14-mer.[37−39] They have been reported to demonstrate an excellent safety profile in human clinical trials as well. Additionally, higher antisense activity of chimeric ASO-(PS-DNA)-ASO/RNA gapmer duplexes has been reported; however, fully modified ASO/RNA duplexes have been considered in the present work to study the influence and differentiate the properties of the

https://doi.org/10.1021/acsomega.2c07860
ACS Omega 2023, 8, 22382−22405

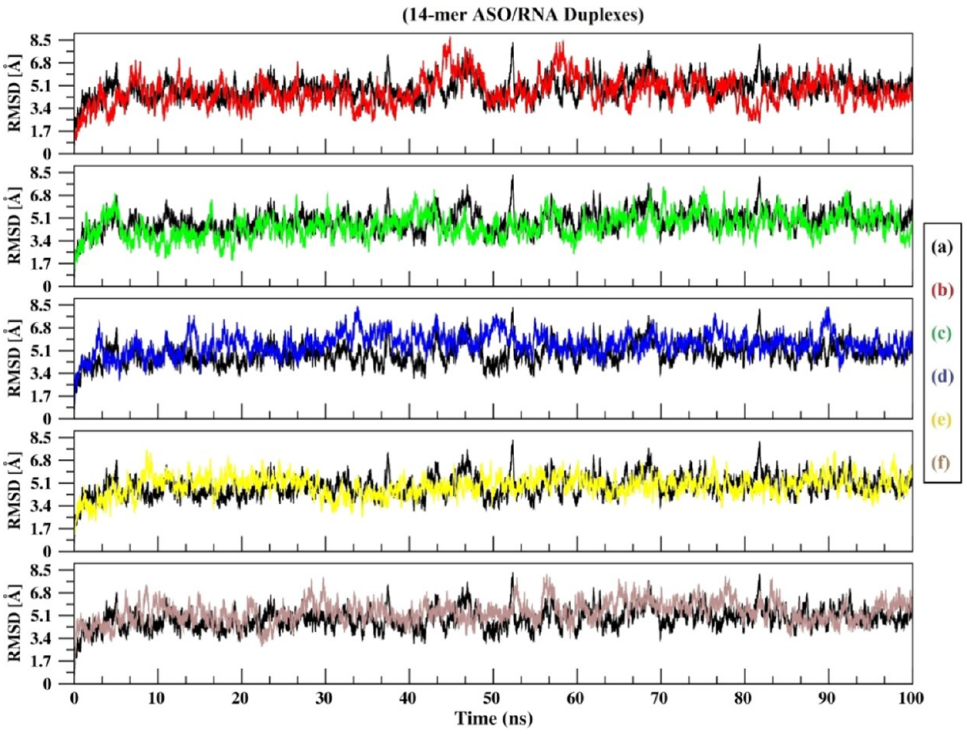

Figure 6. RMSD plots of the 14-mer ASO/RNA duplexes (a) LNA/RNA, (b) A1/RNA, (c) A2/RNA, (d) A3/RNA, (e) A4/RNA, and (f) A5/RNA for the entire simulation trajectory.

proposed modifications over parent LNA ASOs and to particularly compare the same with already reported fully modified LNA/RNA duplexes.

Structures of the 14-mer ASO/RNA duplexes (a) LNA/RNA, (b) A1/RNA, (c) A2/RNA, (d) A3/RNA, (e) A4/RNA, and (f) A5/RNA considered for the simulation study are shown in Figure 5. Since the modifications are LNA-based, a fully modified LNA/RNA hybrid has been considered the control system for comparison. All the six duplexes were observed to be right-handed trying to adopt typical *A-form* duplex configurations. The modified 2′C-4′C bridges were located toward the edge of the minor groove with no steric hindrance for duplex formation. The *N*-glycosidic dihedral angles were in the *anti*-conformation, maintaining stable *Watson−Crick* base pairing for all the base pairs throughout the duplex. An identical base stacking pattern was also observed for all the ASO/RNA duplexes similar to that of the LNA/RNA control system. Thus, the base pairing and base stacking patterns were not altered by incorporation of the proposed antisense modifications. The overall appearance of the duplexes was right-handed helical with apparent *Watson−Crick* base pairing and base stacking patterns and all participating nucleotides in *anti*-conformations well described in the subsequent sections.

Structures obtained from the entire simulation trajectory were then compared with their respective initial structures by analyzing their RMSD plots presented covering the entire duplex, plotted in Figure 6 with RoG plots in Figure S3 (SI). Information of RMSD versus time for the ASO/RNA duplexes showed that duplex stability is well maintained for the entire simulation time in each case. Visual inspection of the trajectories showed that each of the duplexes was fluctuating potentially in and around a range of 2−5 Å of RMSD values. Earlier simulation studies on 14-mer gapmer duplexes with LNA and MOE modifications depicted RMSDs of ∼2−6 Å for complete duplexes and ∼1−3 Å for the nonterminal base pairs.[45] The calculated average RMSD values of the LNA-containing duplexes exhibited an average RMSD of 4.87 Å and duplexes containing modifications A1, A2, A3, A4, and A5 exhibited average RMSDs of 4.64, 4.52, 5.60, 4.89, and 5.36 Å, respectively. A1/RNA and A2/RNA duplexes exhibited relatively lower RMSDs and A3/RNA, A4/RNA, and A5/RNA duplexes exhibited relatively higher RMSDs compared to those of the LNA/RNA control system. From the overall results, it was observed that the modified ASO/RNA duplexes in the present study exhibited stable RMSDs compared to those of the reported LNA- and MOE-containing ASO/RNA hybrids.

3.2.2. Oligomer Duplex Dynamic Structure: Interstrand and Intrastrand Phosphate−Phosphate (PP) Distances. The structural framework of nucleic acid duplexes comprises two sugar/phosphate backbones twisted together to form the molecular double helix. The *C2′-endo* sugar puckering seen in *B-type* duplexes is described by longer intrastrand phosphate−phosphate (PP) distances (∼7 Å), while the *C3′-endo* sugar puckering seen in *A-type* duplexes is described by lower intra-PP distances (∼5.9 Å).[75,76] Average inter-PP and intra-PP distances of the modified ASO/RNA duplexes for both the strands for the entire simulation trajectory are plotted in Figure 7. Monomer nucleotides from the LNA/RNA duplex exhibited intra-PP distance of <6.2 Å for the RNA strand residues and ∼6.8 Å for the LNA strand residues. For the ASO/RNA duplexes, the RNA strand residues exhibited highly flexible intra-PP distances ranging from ∼5.8 to 6.9 Å, and in a similar way, nucleotide residues from the ASO strands also exhibited variable intra-PP distances ranging from ∼5.1 to 6.8 Å.

3.2.3. Torsion Angle Dynamics: Sugar Pucker and N-Glycosidic Torsion Angle Distribution. Base pairing and base

https://doi.org/10.1021/acsomega.2c07860
ACS Omega 2023, 8, 22382−22405

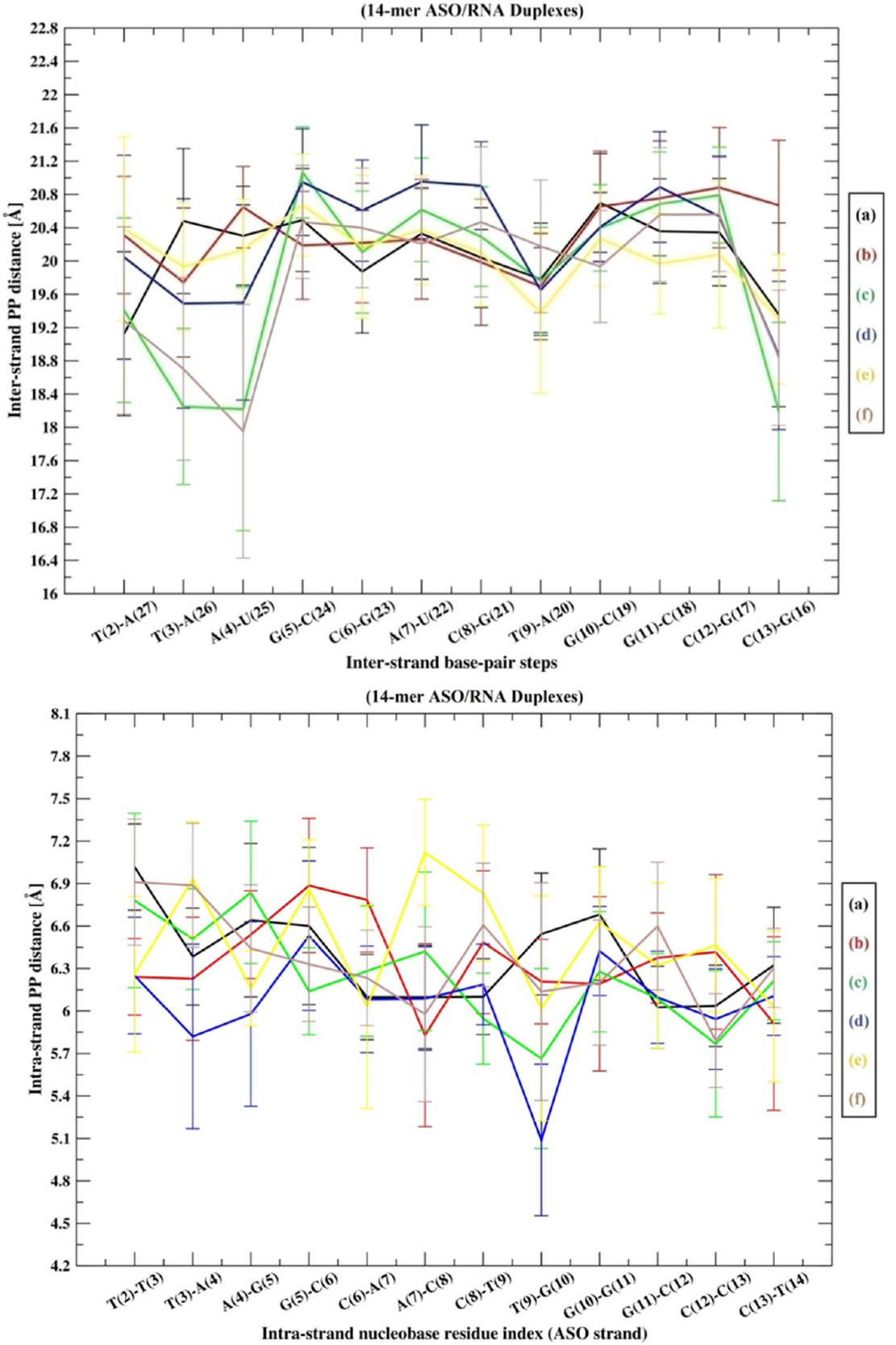

Figure 7. continued

https://doi.org/10.1021/acsomega.2c07860
ACS Omega 2023, 8, 22382−22405

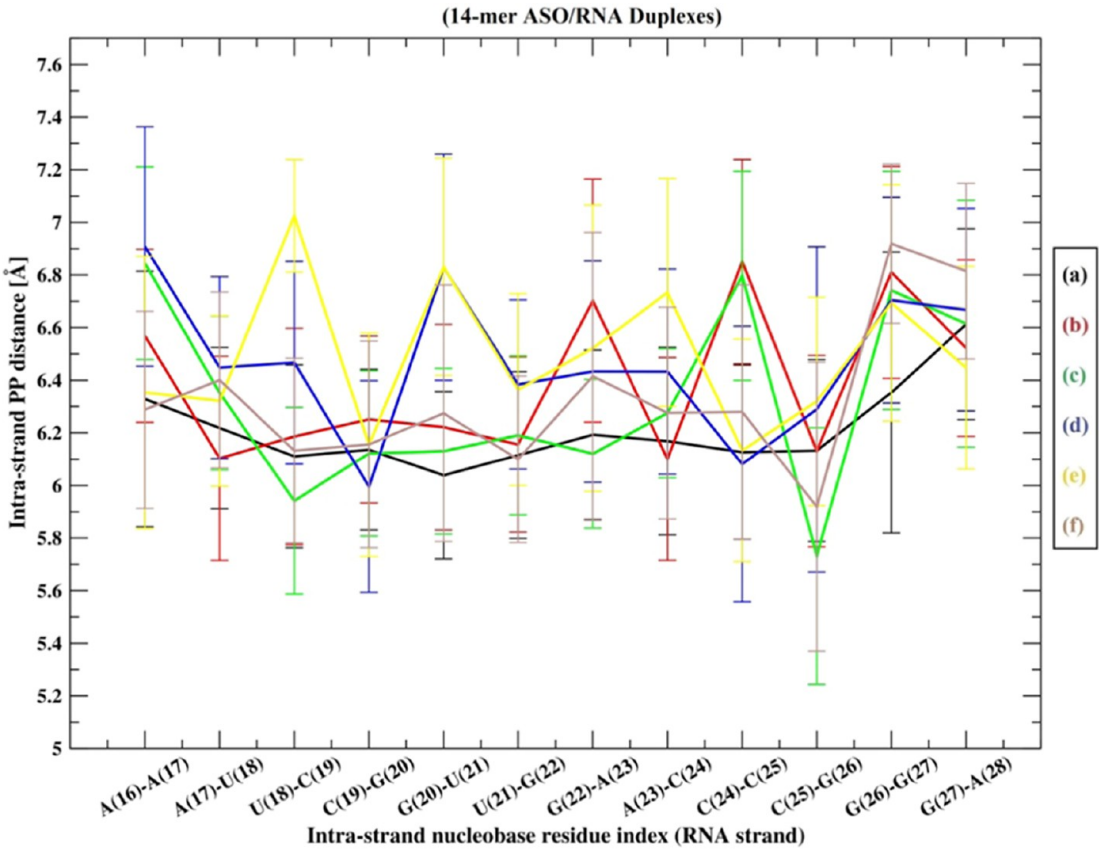

Figure 7. Interstrand and intrastrand PP distances of the 14-mer ASO/RNA duplexes (a) LNA/RNA, (b) A1/RNA, (c) A2/RNA, (d) A3/RNA, (e) A4/RNA, and (f) A5/RNA for both the strands for the entire simulation trajectory.

stacking are directly correlated with the sugar puckering distribution of the nucleotides and accordingly upon the orientation of the phosphate backbone relative to the sugar or the nucleobases. Differences in nonbonded conflicts caused by the *C2′-endo* versus *C3′-endo* conformations are clearly reflected in the correlations between the nucleotide sugar puckering and *N-glycosidic* dihedral angles. Nucleic acids contain sugar puckers that are either in the *C3′-endo* (pucker-phase values: 0−40°) or the *C2′-endo* (pucker-phase values: 120−180°) conformations, which correspond to the *A-form* or *B-form* conformations in a duplex, respectively. According to earlier NMR structures and MD simulation studies on LNA ASOs, LNA steers a larger population of the sugar puckers to the *C3′-endo* conformation in an effort to create an overall *A-form* geometry. To predict the magnitude of such conformational integration of the modified LNA ASOs, sugar pucker distribution of the nucleotide residues throughout the duplex for the modified ASO/RNA duplexes is plotted in Figure 8. As seen in Figure 8, sugar puckers of all the nucleotides from the ASO strand lie in the range of 0−40°, inferring that the nucleotides were in the C3′-*endo* conformation throughout the simulation period. As for the RNA strands, although majority of the residues were exhibiting the *C3′-endo* conformation, a few were seen to fluctuate from the ideal *C3′-endo* conformation, exhibiting a conformation in between *C3′-endo* and *C2′-endo* conformations. Thus, residues from the ASO strands containing the proposed LNA analogue antisense modifications are clearly visible influencing the sugar puckering pattern on their complementary RNA strands.

The *N-glycosidic* dihedral angle measures the influence of the modifications on the distance between the atoms bonded directly to the C1′ carbon that forms the glycosidic bond with RNA. The *N-glycosidic* bond and the corresponding chi (χ) torsion angle illustrate that the nucleobase and sugar are two separate entities and that there is an internal degree of freedom between them. The *N-glycosidic* dihedral angle chi (χ) was calculated to explore the rigidity and dependency of each modified nucleotide on the sugar/nucleobase orientation such that the modified nucleotides exist in an *anti*-conformation, a property of the *A-form* helix observed in RNAs. Although chi (χ) is capable of adopting a large range of values, structural restrictions limit the values for well-defined preferences. It has been already discussed that the chi (χ) torsion angle defined by the O4′-C1′-N9-C4 atoms for purines and O4′-C1′-N1-C2 atoms for pyrimidines specifies the relative sugar/nucleobase orientation in standard nucleic acids. Two main low-energy conformations for the *A-form* and *B-form* duplexes were predicted by theory in accordance with experimental results, where ranges of +90 to +180° and −90 to −180° (or 180 to 270°) correspond to the *anti*-conformation and values in the range of −90 to +90° correspond to the *syn*-conformation. The syn-glycosidic angles are uncommon in nucleotides with C3′-endo sugar puckers due to the steric conflict between the nucleobase and the H3′ atom, which is pointed toward the base in this specific pucker mode. To explore the rigidity of the nucleotide residues throughout the duplex, *N-glycosidic* torsion distribution of the monomer nucleotides from both the strands of the ASO/RNA duplexes is plotted in Figure 9. As seen in Figure 9, the monomer nucleotides from the modified ASO/

https://doi.org/10.1021/acsomega.2c07860
ACS Omega 2023, 8, 22382−22405

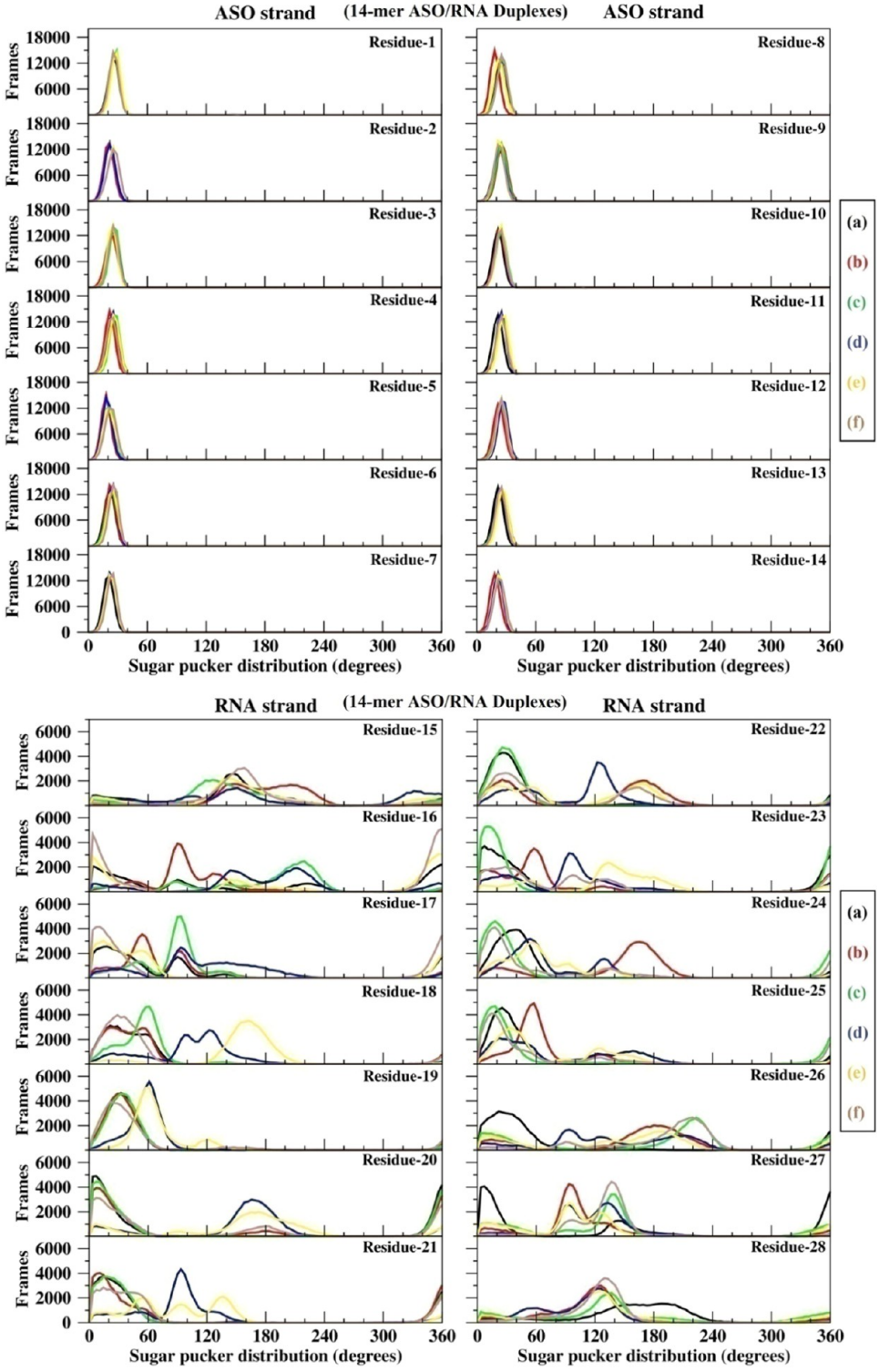

Figure 8. Sugar puckering of the 14-mer ASO/RNA duplexes (a) LNA/RNA, (b) A1/RNA, (c) A2/RNA, (d) A3/RNA, (e) A4/RNA, and (f) A5/RNA for the entire simulation trajectory.

RNA duplexes exhibited chi (χ) values strictly ranging between −120 and −180° for the ASO strand residues and values ranging from −60 to −180° for the RNA strand residues. Although residues from the ASO strands containing the proposed LNA analogue antisense modifications were seen influencing the *N-glycosidic* torsion distribution on their complementary RNA strands, the duplexes were trying to maintain their relative sugar/base orientations to be in the *anti*-conformation, maintaining stable *Watson−Crick* base pairing throughout the duplex for the entire simulation time.

3.2.4. Backbone Flexibility, Base Pairing, Base Stacking, and H-Bond Interactions. The sugar/phosphate backbone of nucleic acid duplexes provides directionality and flexibility to the nucleotides throughout the duplex. Now, flexibility of the sugar/phosphate backbone is reported to play a major role in human RNase H recognition of antisense duplexes. The active

https://doi.org/10.1021/acsomega.2c07860
ACS Omega 2023, 8, 22382−22405

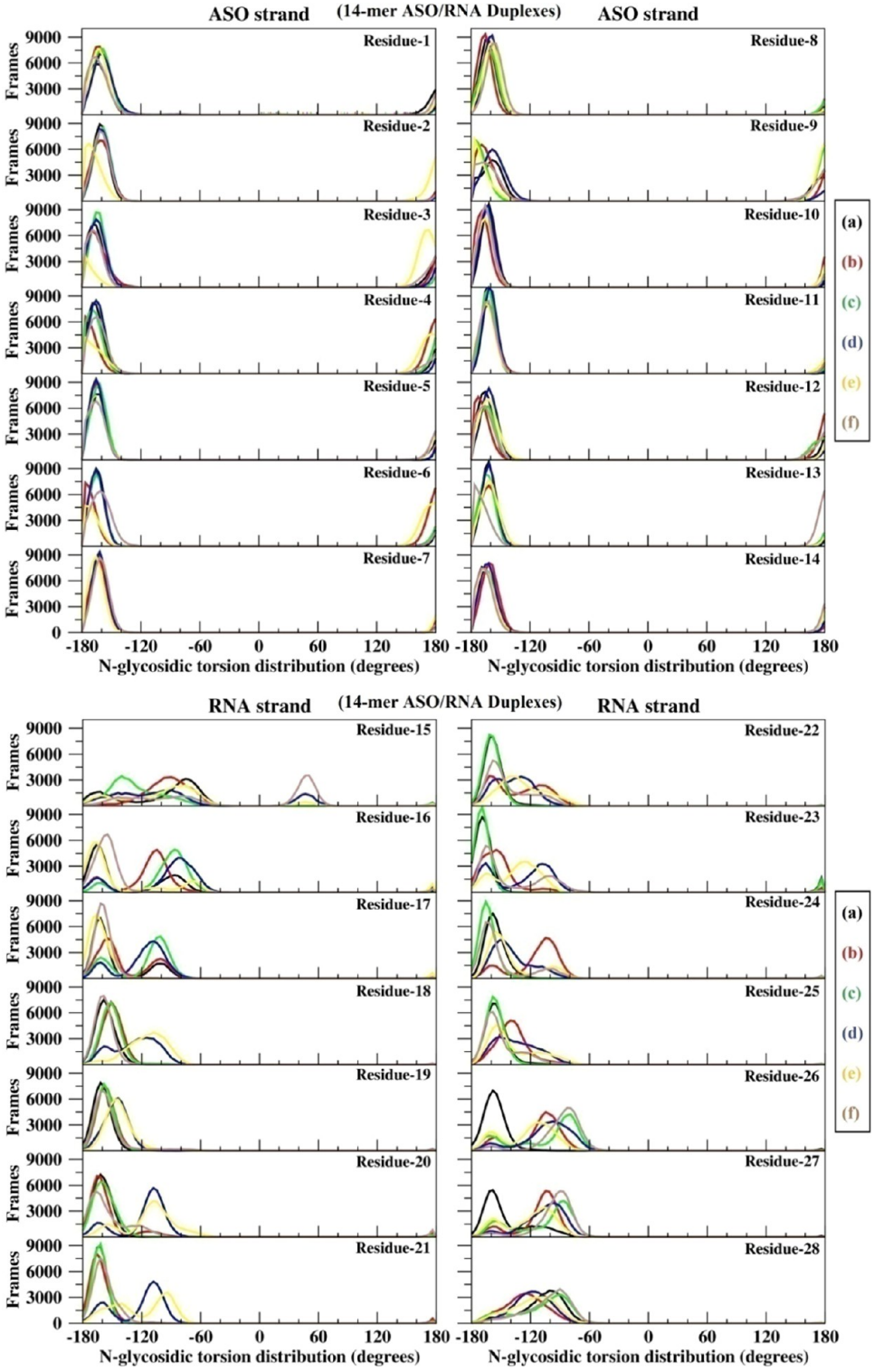

Figure 9. *N*-Glycosidic dihedral of the 14-mer ASO/RNA duplexes (a) LNA/RNA, (b) A1/RNA, (c) A2/RNA, (d) A3/RNA, (e) A4/RNA, and (f) A5/RNA for the entire simulation trajectory.

site of the enzyme comprises an RNA-binding groove and a spatially conserved phosphate-binding pocket, which defines a DNA-binding site. Specific binding of the DNA/RNA duplexes is highly dependent on the surface complementarity and close fitting of the sugar/phosphate backbone of the DNA, making *van der Waals* contacts and H-bond interactions at the active site of RNase H. Depending on the flexibility of the backbone, the minor groove width of the DNA/RNA duplexes changes at the phosphate-binding pocket of the DNA-binding channel. Backbone flexibility thus plays a significant role in imparting dominant antisense activity when it comes to modified ASO/RNA duplexes. Fully modified LNA duplexes are reported to exhibit low backbone flexibility and to not force their flexibility on their complementary partner strands. To explore the influence of the proposed modifications on the duplex backbone flexibility, residuewise RMSF of backbone heavy

https://doi.org/10.1021/acsomega.2c07860
ACS Omega 2023, 8, 22382−22405

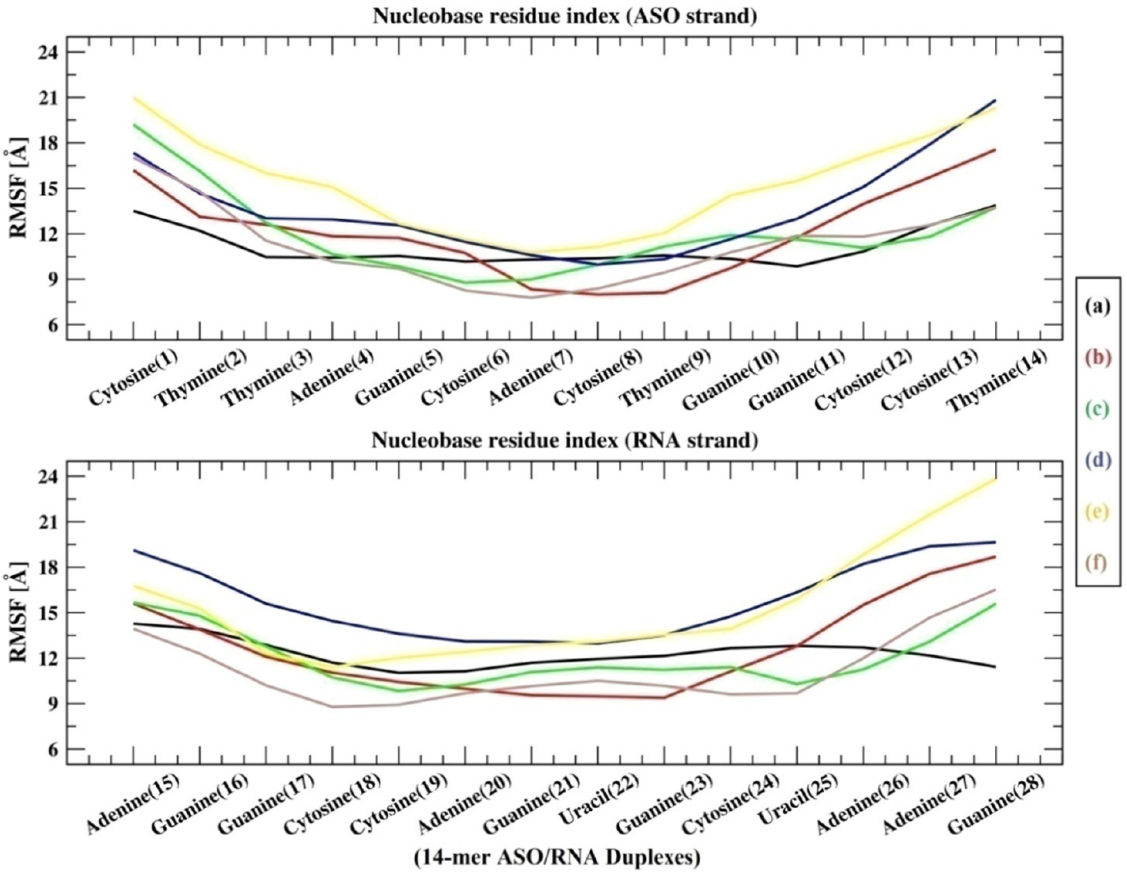

Figure 10. Backbone flexibility of monomer nucleotides of the 14-mer ASO/RNA duplexes (a) LNA/RNA, (b) A1/RNA, (c) A2/RNA, (d) A3/RNA, (e) A4/RNA, and (f) A5/RNA for both the antisense and sense strands for the entire simulation trajectory.

atoms was calculated for each nucleotide from both the nucleic acid strands plotted in Figure 10. In general nucleic acid duplexes, the terminal residues show high fluctuations compared to the nonterminal residues. Accordingly, terminal residues of the ASO/RNA duplexes demonstrated high fluctuations compared to the nonterminal residues. Comparing the nonterminal residues of all the duplexes, the A1-, A2-, and A5-modified ASO strands influenced their complementary RNA strands such that both the strands exhibited low backbone flexibility compared to that of the LNA/RNA duplex. However, A3/RNA and A4/RNA exhibited higher flexibility compared to that of the LNA/RNA control system for both the sense and antisense strands, thus suggesting these modifications to be highly flexible compared to the parent LNA modification, thus serving the very purpose of its creation.

Base pairing is immensely essential for functional RNAs, as the folded structures of the RNA molecules are highly stabilized by their base pairing interactions, which utilize the 2′-OH group of the ribose sugar ring.[77,78] The proposed modifications being 2′-OH-modified would thus affect the active base-pairing conformations of the modified ASO/RNA duplexes. To bind sequence-specifically to their target RNAs, the modified monomer nucleotides should form effective base pairing with the RNA nucleotides, for which the same should exist in an *anti*-conformation, a property of the *A-form* helix generally observed in RNAs.[79] Also, the modified nucleotides in complex with the RNAs should induce the RNA nucleotides to adopt or retain an *N-type* conformation favoring *C3′-endo* sugar puckering, which will reduce the conformational flexibility of the ribose sugar and increase the local organization of the phosphate backbone. The base-pairing pattern is well maintained for all the ASO/RNA duplexes including the LNA/RNA control system with an optimum width of 11−12 Å, plotted in Figure S4 (SI). Because we have observed that the systems formed stable duplexes, we expect the base pairing and base stacking values to be close to the canonical reference values of standard nucleic acid duplexes.[80] Base pair parameters such as shear, stretch, stagger, buckle, propeller, and opening and the base pair step parameters such as shift, slide, rise, tilt, roll, and twist have been calculated for all the duplexes and are listed in Tables S3 and S4 (SI), respectively. Helicoidal parameters such as x-displacement, y-displacement, rise, inclination, tip, and twist all were calculated and are listed in Table S5 (SI). Positive values of X-displacement indicate the helix axis passing by the major groove, whereas a negative value indicates the helix passing by the minor groove of the base pairs. In general, the X-displacement is negative for *A*-form duplexes like the RNAs or *A*-DNAs and Y-displacement is ∼0 for both *A*-form and *B*-form duplexes. X-displacement in the modified ASO/RNA duplexes is negative. Rise values are ∼2.5 Å for *A*-form duplexes and ∼3.38 Å for *B*-form duplexes. In our duplexes, the rise values are concentrated in between ∼1 and ∼2.5 Å. Twist values are 32 for *A*-form duplexes and 36 for *B*-form duplexes. In our duplexes, the twist values are majorly below 34.

Noting the importance of H-bonding and base pairing interactions, the interstrand H-Bond distances, bond angles, and bond residence frames for the ASO/RNA duplexes are calculated and plotted in Table S6 (SI). The % fraction of

https://doi.org/10.1021/acsomega.2c07860
ACS Omega 2023, 8, 22382−22405

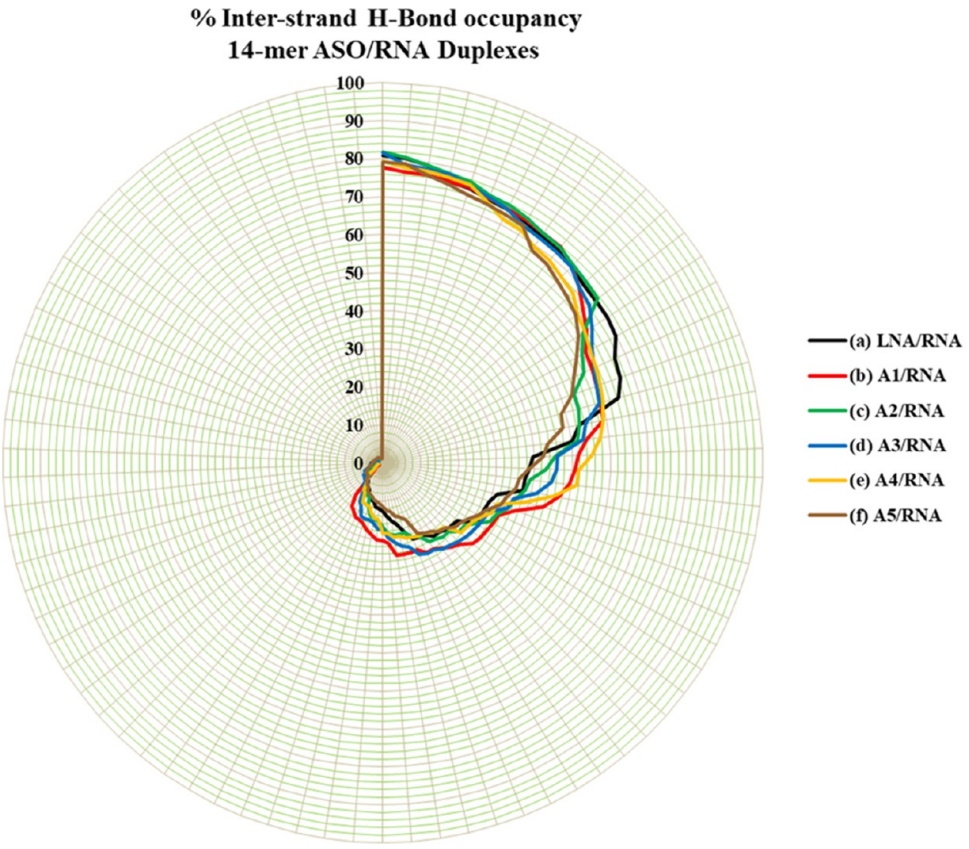

Figure 11. % Occupancy of interstrand H-Bonds of the 14-mer ASO/RNA duplexes (a) LNA/RNA, (b) A1/RNA, (c) A2/RNA, (d) A3/RNA, (e) A4/RNA, and (f) A5/RNA for the entire simulation trajectory.

Table 3. SASA and MM-GBSA Free Energies of the 14-mer ASO/RNA Duplexes (a) LNA/RNA, (b) A1/RNA, (c) A2/RNA, (d) A3/RNA, (e) A4/RNA, and (f) A5/RNA for the Entire Simulation Trajectory

		MM-GBSA (kcal/mol)			
ASO/RNA duplexes	SASA (Å^2)	$G_{ASO/RNA}$	G_{RNA}	G_{ASO}	ΔG
(a) LNA/RNA	5966.939	−4075.61	−1876.88	−2084.73	−113.98
(b) A1/RNA	5841.794	−3474.70	−1274.21	−2088.58	−111.90
(c) A2/RNA	6224.247	−3571.79	−1360.86	−2095.24	−115.68
(d) A3/RNA	6396.581	−3705.86	−1499.91	−2091.72	−114.21
(e) A4/RNA	6330.429	−3848.07	−1657.60	−2084.94	−105.52
(f) A5/RNA	6314.375	−3928.79	−1724.63	−2097.86	−106.29

interstrand H-Bonds formed throughout the simulation time is plotted in Figure 11. All the base pairs exhibited interstrand H-Bond distances of ∼2.7 to ∼2.9 Å, thus maintaining stable *Watson−Crick* base pairing for the complete simulation trajectory. H-Bond parameters are in good agreement with the crystal data values corresponding to the *A*-form duplex structure of RNAs.[80]

3.2.5. SASA and MM-GBSA Binding Free Energy of the Modified ASO/RNA Duplexes. Solvent-accessible surface area (SASA) and MM-GBSA binding free energy have always been considered decisive factors in research on protein folding and on drug−protein stability. Accordingly, the SASA and MM-GBSA free energy of the modified ASO/RNA duplexes can play an important role in understanding the solvation pattern, including the stability of the duplexes. Thus, solvation energies of all the six duplexes were evaluated by calculating their SASA values considering the entire simulation trajectory, enlisted in Table 3. Higher aqueous solubility of the LNA antisense modifications has already been reported. Accordingly, results of SASA values revealed that solvation of all the duplexes comprising A2/RNA, A3/RNA, A4/RNA, and A5/RNA was even higher than that of the LNA/RNA control system.

It has already been predicted from the monomer level studies that both purine and pyrimidine nucleobases bearing modifications A3, A4, and A5 will be more inclined to donate as well as accept electrons compared to those with modifications A1 and A2. Also, the molecular MO analysis predicted MO isosurfaces for both purines and pyrimidines to be majorly distributed on the nucleobase region for modifications A1 and A2 and in the bridging unit in the case of modifications A3, A4, and A5. Results from the various global reactivity descriptors also suggested that modifications A3, A4, and A5 will be more active in electron receiving and elimination processes during a chemical reaction and are expected to interact more with their surrounding environment including the cellular endonuclease RNase H compared to modifications A1 and A2 irrespective of the type of nucleobase, be it the purines or the pyrimidines. Relating the monomer

https://doi.org/10.1021/acsomega.2c07860
ACS Omega 2023, 8, 22382−22405

conformational effects to the behavior of these modifications at the oligomer level suggests the A3/RNA, A4/RNA, and A5/RNA duplexes compared to the A1/RNA and A2/RNA duplexes to be highly available to the surrounding environment for various electron exchange processes, which may aid in the interaction with the RNase H and solvent environment and thereby increase their antisense activity. Accordingly, results from the SASA values revealed that solvation of A3/RNA, A4/RNA, and A5/RNA duplexes was higher compared to that of LNA/RNA, A1/RNA, and A2/RNA duplexes, as their MO isosurfaces were located on the bridging units, which were highly available for solvation.

MM-GBSA is a post-simulation analysis method usually used to evaluate binding free energies or to calculate absolute free energies of molecules in solution. We have calculated the MM-GBSA free energy values of all the duplexes for the entire simulation trajectory, computed with the equation

$$\Delta G_{\text{binding}} = G_{\text{ASO/RNA}} - G_{\text{ASO}} - G_{\text{RNA}}$$

Herein, the energies were calculated by considering the RNA strand as the target receptor, the ASO strand containing the modified nucleotides as binding ligands, and ASO/RNA duplexes as the receptor−ligand complex molecule. The average MM-GBSA binding free energy values from the entire simulation trajectory are listed in Table 3. G_{RNA} energy of the RNA strand has almost similar values for all the duplexes. The modified ASO strand on the other hand has different G_{ASO} energy values depending on the type of modifications. As seen in Table 3, although the $G_{\text{ASO/RNA}}$ energy values of the duplexes were less, A3/RNA, A4/RNA, and A5/RNA duplexes have the most nearest values compared to that of the control LNA/RNA system. On the other hand, although A1/RNA, A2/RNA, and A3/RNA have lower $G_{\text{ASO/RNA}}$ energy values, the ΔG of the same has the most nearest values compared to that of the LNA/RNA control system. In fact, the A2/RNA and A3/RNA duplexes have higher ΔG values compared to that of the LNA/RNA control system. Thus, the MM-GBSA binding energies of the modified ASO/RNA duplexes containing the proposed LNA analogue antisense modifications estimated for the entire simulation trajectory were predicted to be equally stable as the LNA/RNA control system.

4. CONCLUSIONS

The present work focuses on performing a detailed quantum chemical study of five novel LNA analogue antisense alterations (A1, A2, A3, A4, A5) and establishing each with the five standard nucleic acids adenine (A), guanine (G), cytosine (C), thymine (T), and uracil (U) at the monomer level using DFT methods and to relate the conformational effects induced by these alterations at the oligomer level using MD simulations studies. Accordingly, we have studied the structural and electronic properties and quantum chemical parameters of the proposed LNA analogue antisense modifications at the monomer level. Oligomer-level hybrid duplex stability containing the modifications is described by performing a detailed MD simulation study by incorporating the modifications onto 14-mer ASO/RNA duplex systems.

According to the monomer-level investigation, there is no disturbance in the *N-type* sugar puckering due to the infusion of the proposed alterations. Also, the relative sugar−base orientation existed in an *anti*-conformation, which can increase the strength of base-pairing and base-stacking interactions preferring RNA-mimicking conformations. Monomer nucleotides with modifications A3, A4, and A5 are predicted to be better electron donors as well as better electron acceptors compared to A1 and A2 for both the purine and pyrimidine nucleobases. HOMO−LUMO isosurfaces of A1 and A2 are majorly distributed on the nucleobase region, whereas for A3, A4, and A5, they are well distributed in the modified bridging unit for both the purine and pyrimidine nucleobases. In A1 and A2, the MO isosurfaces being embedded in the nucleobase region might decrease their possibility of interactions with the RNase H and solvent environment. On the contrary, in A3, A4, and A5, the MO isosurfaces being well distributed in the modified bridging unit will be highly available to the surrounding environment for various electron exchange processes, which may aid in the interaction with the RNase H and solvent environment and thereby increase their antisense activity.

Furthermore, derivation of the global reactivity descriptors global hardness (η), global softness (S), chemical potential (μ), and electrophilicity (ω) of the monomer nucleotides has helped in understanding the dependency of their electronic properties with varying structural modifications. Global hardness and softness suggest that modifications A3, A4, and A5 will be more active in electron receiving and elimination processes or softer during a chemical reaction compared to modifications A1 and A2 irrespective of the type of nucleobase, be it the purines or the pyrimidines. Chemical potential results suggest that A1, A2, and A5 have more negative chemical potential values and A3 and A4 have less negative chemical potential values for the purines; A1 and A2 have more negative chemical potential values and A3, A4, and A5 have less negative chemical potential values for the pyrimidines. Electrophilicity results suggest that A3 and A4 are less electrophilic, while A1, A2, and A5 are more electrophilic irrespective of the type of nucleobases, be it the purines or the pyrimidines. This is an implication of A3 and A4 having high-lying E_{HOMO}, which will accept electrons less easily rather than donating more easily, hence being less electrophilic, compared to A1, A2, and A5 having low-lying E_{HOMO}, which will donate electrons less easily, rather than accepting more easily, hence being more electrophilic. Overall, modifications A3 and A4 have less negative chemical potential and are less electrophilic compared to modifications A1, A2, and A5 for both the purine and pyrimidine nucleobases. Such small changes in the values of the descriptors may be useful in capturing differences between the proposed antisense modifications at the monomer level, which may contribute to understanding the behavior of these modifications at the oligomer level.

According to the oligomer-level investigation, the 2′carbon and 4′carbon bridges in the modified ASO/RNA duplexes were located toward the edge of the minor groove maintaining stable helical structures. The oligomer duplex structure, sugar puckering, *N*-glycosidic torsion angle distributions, backbone conformation, base pairing, base stacking, H-bond distances, and base pair distances all were in accordance, trying to adopt a right-handed *A-form* helix preferring RNA-mimicking *A-form* geometries, which can increase the strength of base pairing and base stacking interactions during duplex formation. The duplexes exhibited stable RMSDs compared to those of the LNA- and MOE-modified hybrids reported in the literature. While structural studies reported low flexibility of fully modified LNA/RNA duplexes, the modified duplexes in our

https://doi.org/10.1021/acsomega.2c07860
ACS Omega 2023, 8, 22382−22405

case exhibited higher flexibility compared to that of the LNA/RNA duplexes, suggesting that these modifications induce higher flexibility compared to that of the parent LNA modification, the very reason for considering fully modified duplexes in the present study.

Monomer-level studies clearly predicted MO surfaces to be majorly distributed on the nucleobase region in A1 and A2 and in the bridging unit in A3, A4, and A5. Results from the various global reactivity descriptors also suggested that compared to A1 and A2 modifications, A3, A4, and A5 will be more active in electron receiving and elimination processes during a chemical reaction and are expected to interact more with their surrounding environment including the cellular endonuclease RNase H. Relating the monomer conformational effects to the behavior of these modifications at the oligomer level suggests that A3/RNA, A4/RNA, and A5/RNA duplexes compared to A1/RNA and A2/RNA duplexes are highly available to the surrounding environment for various electron exchange processes, which may aid in the interaction with the RNase H and solvent environment and thereby increase their antisense activity. Accordingly, solvation of A3/RNA, A4/RNA, and A5/RNA duplexes was higher compared to that of LNA/RNA, A1/RNA, and A2/RNA duplexes, as their MO isosurfaces located on the bridging units were highly available for solvation. This study has resulted in a successful archetype for creating advantageous nucleic acid modifications tailored for particular needs in designing novel antisense modifications that may overcome the drawbacks and improve the pharmacokinetics of existing LNA antisense modifications.

■ ASSOCIATED CONTENT

Supporting Information

The Supporting Information is available free of charge at https://pubs.acs.org/doi/10.1021/acsomega.2c07860.

Calculated IR spectra, molecular orbital (MO) analysis, global hardness (η), global softness (S), chemical potential (μ), and electrophilicity (ω) plots and values of the proposed LNA analogue antisense modifications A1, A2, A3, A4, and A5 with their respective nucleobases adenine (A), guanine (G), cytosine (C), thymine (T), and uracil (U) calculated at the M06-2X/6-311G(d,p) level of theory; RoG plot, base pair distances, base pair parameters, base pair step parameters, helix parameters, and interstrand H-bond distance, bond angle, and bond residence frames of the 14-mer ASO/RNA duplexes LNA/RNA, A1/RNA, A2/RNA, A3/RNA, A4/RNA, and A5/RNA for the entire simulation 100 ns trajectory; coordinates of optimized structures of the monomer nucleotides of the proposed LNA analogue antisense modifications A1, A2, A3, A4, and A5 with their respective nucleobases adenine (A), guanine (G), cytosine (C), thymine (T), and uracil (U) calculated at the M06-2X/6-311G(d,p) level of theory; and Frcmod and library files of the proposed LNA analogue antisense modifications A1, A2, A3, A4, and A5 with their respective nucleobases adenine (A), guanine (G), cytosine (C), thymine (T), and uracil (U) used in the simulation studies (PDF)

Molecular orbital (MO) analysis; base pair parameters; base pair step parameters, helix parameters, and interstrand H-Bond distance, bond angle, and bond residence frames (XLSX)

■ AUTHOR INFORMATION

Corresponding Author

Ramesh Ch. Deka − *CMML—Catalysis and Molecular Modelling Lab, Department of Chemical Sciences, Tezpur University, Sonitpur, Assam 784 028, India; Center for Multidisciplinary Research, Tezpur University, Sonitpur, Assam 784028, India;* orcid.org/0000-0003-4352-2661; Email: ramesh@tezu.ernet.in

Authors

Dikshita Dowerah − *CMML—Catalysis and Molecular Modelling Lab, Department of Chemical Sciences, Tezpur University, Sonitpur, Assam 784 028, India*

Mallikarjunachari V. N. Uppuladinne − *HPC—Medical & Bioinformatics Applications Group, Centre for Development of Advanced Computing (C-DAC), Pune 411008, India*

Plaban J. Sarma − *CMML—Catalysis and Molecular Modelling Lab, Department of Chemical Sciences, Tezpur University, Sonitpur, Assam 784 028, India; Department of Chemistry, Gargaon College, Sivasagar, Assam 785685, India;* orcid.org/0000-0002-2457-1559

Nishant Biswakarma − *CMML—Catalysis and Molecular Modelling Lab, Department of Chemical Sciences, Tezpur University, Sonitpur, Assam 784 028, India*

Uddhavesh B. Sonavane − *HPC—Medical & Bioinformatics Applications Group, Centre for Development of Advanced Computing (C-DAC), Pune 411008, India*

Rajendra R. Joshi − *HPC—Medical & Bioinformatics Applications Group, Centre for Development of Advanced Computing (C-DAC), Pune 411008, India;* orcid.org/0000-0003-1299-0091

Suvendra K. Ray − *Department of Molecular Biology and Biotechnology and Center for Multidisciplinary Research, Tezpur University, Sonitpur, Assam 784028, India*

Nima D. Namsa − *Department of Molecular Biology and Biotechnology and Center for Multidisciplinary Research, Tezpur University, Sonitpur, Assam 784028, India;* orcid.org/0000-0002-9412-8915

Complete contact information is available at: https://pubs.acs.org/10.1021/acsomega.2c07860

Author Contributions

D.D.: conceptualization, data curation, formal analysis, data investigation, interpretation, and writing—original draft. M.V.N.U.: conceptualization, data investigation, interpretation, and writing—original draft. P.J.S. and N.B.: formal analysis, data investigation, and interpretation, U.B.S., R.R.J., S.K.R., N.D.N., and R.Ch.D.: resources, project administration, fund acquisition, and review and editing the article.

Notes

The authors declare no competing financial interest.

■ ACKNOWLEDGMENTS

This work was financially supported by the Department of Biotechnology (DBT), Government of India (Project No. BT/PR16182/NER/95/92/2015). P.J.S. is thankful to the Science and Engineering Research Board (SERB) (Project No. EMR/2016/003195). N.B. is thankful to the Department of Science and Technology (DST) Nanomission, Government of India, Project No. SR/NM/NS-1147/2016(G). D.D. acknowledges the Tezpur University supercomputing facility PARAMTEZ. M.V.N.U. acknowledges the National Supercomputing Mission

https://doi.org/10.1021/acsomega.2c07860
ACS Omega 2023, 8, 22382−22405

(NSM), India, the Ministry of Electronics and Information Technology (MeitY), Government of India, and the Bioinformatics Resources and Applications Facility (BRAF) of C-DAC, Pune.

REFERENCES

(1) Chan, J. H.; Lim, S.; Wong, W. F. Antisense oligonucleotides: from design to therapeutic application. *Clin. Exp. Pharmacol. Physiol.* **2006**, *33*, 533−540.
(2) *Antisense Drug Technology: Principles, Strategies, and Applications*, Crooke, S. T., Ed.; CRC Press, 2007.
(3) Bennett, C. F.; Swayze, E. E. RNA targeting therapeutics: molecular mechanisms of antisense oligonucleotides as a therapeutic platform. *Annu. Rev. Pharmacol. Toxicol.* **2010**, *50*, 259−293.
(4) Zamaratski, E.; Pradeepkumar, P. I.; Chattopadhyaya, J. A critical survey of the structure-function of the antisense oligo/RNA hetero duplex as substrate for RNase H. *J. Biochem. Biophys. Methods* **2001**, *48*, 189−208.
(5) Nowotny, M.; Gaidamakov, S. A.; Ghirlando, R.; Cerritelli, S. M.; Crouch, R. J.; Yang, W. Structure of human RNase H1 complexed with an RNA/DNA hybrid: insight into HIV reverse transcription. *Mol. Cell* **2007**, *28*, 264−276.
(6) Herbert, C.; Dzowo, Y. K.; Urban, A.; Kiggins, C. N.; Resendiz, M. J. Reactivity and specificity of RNase T1, RNase A, and RNase H toward oligonucleotides of RNA containing 8-Oxo-7, 8-dihydroguanosine. *Biochemistry* **2018**, *57*, 2971−2983.
(7) Kiełpiński, Ł. J.; Hagedorn, P. H.; Lindow, M.; Vinther, J. RNase H sequence preferences influence antisense oligonucleotide efficiency. *Nucleic Acids Res.* **2017**, *45*, 12932−12944.
(8) Hagedorn, P. H.; Pontoppidan, M.; Bisgaard, T. S.; Berrera, M.; Dieckmann, A.; Ebeling, M.; Møller, M. R.; Hudlebusch, H.; Jensen, M. L.; Hansen, H. F.; Koch, T.; Lindow, M. Identifying and avoiding off-target effects of RNase H-dependent antisense oligonucleotides in mice. *Nucleic Acids Res.* **2018**, *46*, 5366−5380.
(9) Campbell, J. M.; Bacon, T. A.; Wickstrom, E. Oligodeoxynucleoside phosphorothioate stability in subcellular extracts, culture media, sera and cerebrospinal fluid. *J. Biochem. Biophys. Methods* **1990**, *20*, 259−267.
(10) Zhang, R.; Diasio, R. B.; Lu, Z.; Liu, T.; Jiang, Z.; Galbraith, W. M.; Agrawal, S. Pharmacokinetics and tissue distribution in rats of an oligodeoxynucleotide phosphorothioate (GEM 91) developed as a therapeutic agent for human immunodeficiency virus type-1. *Biochem. Pharmacol.* **1995**, *49*, 929−939.
(11) Agrawal, S.; Goodchild, J.; Civeira, M.; Sarin, P. S.; Zamecnik, P. C. Phosphoramidate, phosphorothioate, and methylphosphonate analogs of oligodeoxynucleotide: inhibitors of replication of human immunodeficiency virus. *Nucleosides, Nucleotides Nucleic Acids* **1989**, *8*, 819−823.
(12) Iwamoto, N.; Butler, D. C.; Svrzikapa, N.; Mohapatra, S.; Zlatev, I.; Sah, D. W.; Standley, S. M.; Lu, G.; Apponi, L. H.; Frank-Kamenetsky, M.; Zhang, J. J.; et al. Control of phosphorothioate stereochemistry substantially increases the efficacy of antisense oligonucleotides. *Nat. Biotechnol.* **2017**, *35*, 845−851.
(13) Shen, W.; De Hoyos, C. L.; Migawa, M. T.; Vickers, T. A.; Sun, H.; Low, A.; Bell, T. A.; Rahdar, M.; Mukhopadhyay, S.; Hart, C. E.; Bell, M.; et al. Chemical modification of PS-ASO therapeutics reduces cellular protein-binding and improves the therapeutic index. *Nat. Biotechnol.* **2019**, *37*, 640−650.
(14) Manoharan, M. 2′-Carbohydrate modifications in antisense oligonucleotide therapy: importance of conformation, configuration and conjugation. *Biochim. Biophys. Acta, Gene Struct. Expression* **1999**, *1489*, 117−130.
(15) Herdewijn, P. Conformationally restricted carbohydrate-modified nucleic acids and antisense technology. *Biochim. Biophys. Acta, Gene Struct. Expression* **1999**, *1489*, 167−179.
(16) Finn, P. J.; Gibson, N. J.; Fallon, R.; Hamilton, A.; Brown, T. Synthesis and properties of DNA-PNA chimeric oligomers. *Nucleic Acids Res.* **1996**, *24*, 3357−3363.
(17) Yu, R. Z.; Kim, T. W.; Hong, A.; Watanabe, T. A.; Gaus, H. J.; Geary, R. S. Cross-species pharmacokinetic comparison from mouse to man of a second-generation antisense oligonucleotide, ISIS 301012, targeting human apolipoprotein B-100. *Drug Metab. Dispos.* **2007**, *35*, 460−468.
(18) Geary, R. S.; Wancewicz, E.; Matson, J.; Pearce, M.; Siwkowski, A.; Swayze, E.; Bennett, F. Effect of dose and plasma concentration on liver uptake and pharmacologic activity of a 2′-methoxyethyl modified chimeric antisense oligonucleotide targeting PTEN. *Biochem. Pharmacol.* **2009**, *78*, 284−291.
(19) Post, N.; Yu, R.; Greenlee, S.; Gaus, H.; Hurh, E.; Matson, J.; Wang, Y. Metabolism and disposition of volanesorsen, a 2′-O-(2 methoxyethyl) antisense oligonucleotide, across species. *Drug Metab. Dispos.* **2019**, *47*, 1164−1173.
(20) Kurreck, J. Antisense technologies: improvement through novel chemical modifications. *Eur. J. Biochem.* **2003**, *270*, 1628−1644.
(21) Moss, K. H.; Popova, P.; Hadrup, S. R.; Astakhova, K.; Taskova, M. Lipid nanoparticles for delivery of therapeutic RNA oligonucleotides. *Mol. Pharmaceutics* **2019**, *16*, 2265−2277.
(22) Gheibi-Hayat, S. M.; Jamialahmadi, K. Antisense Oligonucleotide (AS-ODN) Technology: Principle, Mechanism and Challenges. *Biotechnol. Appl. Biochem.* **2021**, *68*, 1086−1094.
(23) Vitravene Study Group. A randomized controlled clinical trial of intravitreousfomivirsen for treatment of newly diagnosed peripheral cytomegalovirus retinitis in patients with AIDS. *Am. J. Ophthalmol.* **2002**, *133*, 467−474.
(24) Le Calvez, H.; Yu, M.; Fang, F. Biochemical prevention and treatment of viral infections−A new paradigm in medicine for infectious diseases. *Virol. J.* **2004**, *1*, 1−6.
(25) Stein, C. A.; Castanotto, D. FDA-approved oligonucleotide therapies in 2017. *Mol. Ther.* **2017**, *25*, 1069−1075.
(26) Silva, A. C.; Lobo, D. D.; Martins, I. M.; Lopes, S. M.; Henriques, C.; Duarte, S. P.; Dodart, J. C.; Nobre, R. J.; Pereira de Almeida, L. Antisense oligonucleotide therapeutics in neurodegenerative diseases: the case of polyglutamine disorders. *Brain* **2020**, *143*, 407−429.
(27) Takei, Y.; Kadomatsu, K.; Yuzawa, Y.; Matsuo, S.; Muramatsu, T. A small interfering RNA targeting vascular endothelial growth factor as cancer therapeutics. *Cancer Res.* **2004**, *64*, 3365−3370.
(28) Gong, M.; Lu, Z.; Fang, G.; Bi, J.; Xue, X. A small interfering RNA targeting osteopontin as gastric cancer therapeutics. *Cancer Lett.* **2008**, *272*, 148−159.
(29) Singh, S. K.; Koshkin, A. A.; Wengel, J.; Nielsen, P. LNA (locked nucleic acids): synthesis and high-affinity nucleic acid recognition. *Chem. Commun.* **1998**, 455−456.
(30) Abdur Rahman, S. M.; Seki, S.; Obika, S.; Yoshikawa, H.; Miyashita, K.; Imanishi, T. Design, Synthesis, and Properties of 2 ‘,4 ‘-BNA^{NC}: A Bridged Nucleic Acid Analogue. *J. Am. Chem. Soc.* **2008**, *130*, 4886−4896.
(31) Shrestha, A. R.; Kotobuki, Y.; Hari, Y.; Obika, S. Guanidine bridged nucleic acid (GuNA): an effect of a cationic bridged nucleic acid on DNA binding affinity. *Chem. Commun.* **2014**, *50*, 575−577.
(32) Langner, H. K.; Jastrzebska, K.; Caruthers, M. H. Synthesis and characterization of thiophosphoramidatemorpholino oligonucleotides and chimeras. *J. Am. Chem. Soc.* **2020**, *142*, 16240−16253.
(33) Fluiter, K.; ten Asbroek, A. L.; de Wissel, M. B.; Jakobs, M. E.; Wissenbach, M.; Olsson, H.; Olsen, O.; Oerum, H.; Baas, F. In vivo tumor growth inhibition and biodistribution studies of locked nucleic acid (LNA) antisense oligonucleotides. *Nucleic Acids Res.* **2003**, *31*, 953−962.
(34) Darfeuille, F.; Hansen, J. B.; Orum, H.; Primo, C. D.; Toulmé, J. J. LNA/DNA chimeric oligomers mimic RNA aptamers targeted to the TAR RNA element of HIV-1. *Nucleic Acids Res.* **2004**, *32*, 3101−3107.
(35) Laxton, C.; Brady, K.; Moschos, S.; Turnpenny, P.; Rawal, J.; Pryde, D. C.; Sidders, B.; Corbau, R.; Pickford, C.; Murray, E. J. Selection, optimization, and pharmacokinetic properties of a novel, potent antiviral locked nucleic acid-based antisense oligomer targeting

https://doi.org/10.1021/acsomega.2c07860
ACS Omega 2023, 8, 22382−22405

hepatitis C virus internal ribosome entry site. *Antimicrob. Agents Chemother.* **2011**, *55*, 3105−3114.
(36) Swayze, E. E.; Siwkowski, A. M.; Wancewicz, E. V.; Migawa, M. T.; Wyrzykiewicz, T. K.; Hung, G.; Monia, B. P.; Bennett, A. C. F. Antisense oligonucleotides containing locked nucleic acid improve potency but cause significant hepatotoxicity in animals. *Nucleic Acids Res.* **2007**, *35*, 687−700.
(37) Seth, P. P.; Siwkowski, A.; Allerson, C. R.; Vasquez, G.; Lee, S.; Prakash, T. P.; Wancewicz, E. V.; Witchell, D.; Swayze, E. E. Short antisense oligonucleotides with novel 2′−4′ conformationaly restricted nucleoside analogues show improved potency without increased toxicity in animals. *J. Med. Chem.* **2009**, *52*, 10−13.
(38) Seth, P. P.; Vasquez, G.; Allerson, C. A.; Berdeja, A.; Gaus, H.; Kinberger, G. A.; Prakash, T. P.; Migawa, M. T.; Bhat, B.; Swayze, E. E. Synthesis and biophysical evaluation of 2′, 4′-constrained 2′ O-methoxyethyl and 2′, 4′-constrained 2′ O-ethyl nucleic acid analogues. *J. Org. Chem.* **2010**, *75*, 1569−1581.
(39) Prakash, T. P.; Siwkowski, A.; Allerson, C. R.; Migawa, M. T.; Lee, S.; Gaus, H. J.; Black, C.; Seth, P. P.; Swayze, E. E.; Bhat, B. Antisense oligonucleotides containing conformationally constrained 2′, 4′-(N-methoxy) aminomethylene and 2′, 4′-aminooxymethylene and 2′-O, 4′-C-aminomethylene bridged nucleoside analogues show improved potency in animal models. *J. Med. Chem.* **2010**, *53*, 1636−1650.
(40) Yamamoto, T.; Yasuhara, H.; Wada, F.; Harada-Shiba, M.; Imanishi, T.; Obika, S. Superior silencing by 2′,4′-BNA^{NC}-based short antisense oligonucleotides compared to 2′,4′-BNA/LNA-based apolipoprotein B antisense inhibitors. *J. Nucleic Acids* **2012**, *2012*, No. 707323.
(41) Natsume, T.; Ishikawa, Y.; Dedachi, K.; Tsukamoto, T.; Kurita, N. DFT study of the electronic properties of DNA−DNA and PNA−DNA double strands. *Int. J. Quantum Chem.* **2006**, *106*, 3278−3287.
(42) Uppuladinne, M. V. N.; Jani, V.; Sonavane, U. B.; Joshi, R. R. Quantum chemical studies of novel 2′-4′ conformationally restricted antisense monomers. *Int. J. Quantum Chem.* **2013**, *113*, 2523−2533.
(43) Bhai, S.; Ganguly, B. Role of backbones on the interaction of metal ions with deoxyribonucleic acid and peptide nucleic acid: A DFT study. *J. Mol. Graphics Modell.* **2019**, *93*, No. 107445.
(44) Uppuladinne, M. V. N.; Sonavane, U. B.; Deka, R. C.; Joshi, R. R. Structural insight into antisense gapmer-RNA oligomer duplexes through molecular dynamics simulations. *J. Biomol. Struct. Dyn.* **2019**, *37*, 2823−2836.
(45) Galindo-Murillo, R.; Cohen, J. S.; Akabayov, B. Molecular dynamics simulations of acyclic analogs of nucleic acids for antisense inhibition. *Mol. Ther.–Nucleic Acids* **2021**, *23*, 527−535.
(46) Hansen, H. F.; Albaek, N.; Hansen, B. R.; Shim, I.; Bohr, H.; Koch, T. In vivo uptake of antisense oligonucleotide drugs predicted by ab initio quantum mechanical calculations. *Sci. Rep.* **2021**, *11*, No. 6321.
(47) Uppuladinne, M. V.; Dowerah, D.; Sonavane, U. B.; Ray, S. K.; Deka, R. C.; Joshi, R. R. Structural Insight into Locked Nucleic Acid based Novel Antisense Modifications: A DFT calculations at monomer and MD simulations at oligomer level. *J. Mol. Graphics Modell.* **2021**, *107*, No. 107945.
(48) *BIOVIA*, DassaultSystèmes, [Discovery Studio], [Client version 19.1.0], DassaultSystèmes: San Diego, 2019.
(49) Frisch, M. J.; Trucks, G. W.; Schlegel, H. B.; Scuseria, G. E.; Robb, M.; Cheeseman, J. R.; Scalmani, G.; Barone, V.; Mennucci, B.; Petersson, G. A.; Nakatsuji, H.; et al. *Gaussian 09*, revision D.01; Gaussian. Inc.: Wallingford, CT, 2009.
(50) Hehre, W. J.; Ditchfield, R.; Pople, J. A. Self-consistent molecular orbital methods. XII. Further extensions of Gaussian-type basis sets for use in molecular orbital studies of organic molecules. *J. Chem. Phys.* **1972**, *56*, 2257−2261.
(51) Hariharan, P. C.; Pople, J. A. The influence of polarization functions on molecular orbital hydrogenation energies. *Theor. Chim. Acta* **1973**, *28*, 213−222.
(52) Zhao, Y.; Truhlar, D. G. The M06 suite of density functionals for main group thermochemistry, thermochemical kinetics, noncovalent interactions, excited states, and transition elements: two new functionals and systematic testing of four M06-class functionals and 12 other functionals. *Theor. Chem. Acc.* **2008**, *120*, 215−241.
(53) Wang, Y.; Verma, P.; Jin, X.; Truhlar, D. G.; He, X. Revised M06 density functional for main-group and transition-metal chemistry. *Proc. Natl. Acad. Sci. U.S.A.* **2018**, *115*, 10257−10262.
(54) Takano, Y.; Houk, K. N. Benchmarking the conductor-like polarizable continuum model (CPCM) for aqueous solvation free energies of neutral and ionic organic molecules. *J. Chem. Theory Comput.* **2005**, *1*, 70−77.
(55) Lu, T.; Chen, F. Multiwfn: a multifunctional wavefunction analyzer. *J. Comput. Chem.* **2012**, *33*, 580−592.
(56) Parr, R. G.; Yang, W. Density functional approach to the frontier-electron theory of chemical reactivity. *J. Am. Chem. Soc.* **1984**, *106*, 4049−4050.
(57) Luo, J.; Xue, Z. Q.; Liu, W. M.; Wu, J. L.; Yang, Z. Q. Koopmans′ theorem for large molecular systems within density functional theory. *J. Phys. Chem. A* **2006**, *110*, 12005−12009.
(58) Vijayaraj, R.; Subramanian, V.; Chattaraj, P. K. Comparison of global reactivity descriptors calculated using various density functionals: a QSAR perspective. *J. Chem. Theory Comput.* **2009**, *5*, 2744−2753.
(59) Cornell, W. D.; Cieplak, P.; Bayly, C. I.; Gould, I. R.; Merz, K. M.; Ferguson, D. M.; Spellmeyer, D. C.; Fox, T.; Caldwell, J. W.; Kollman, P. A. A second generation force field for the simulation of proteins, nucleic acids, and organic molecules. *J. Am. Chem. Soc.* **1995**, *117*, 5179−5197.
(60) Pérez, A.; Marchán, I.; Svozil, D.; Sponer, J.; Cheatham, T. E., III; Laughton, C. A.; Orozco, M. Refinement of the AMBER force field for nucleic acids: improving the description of α/γ conformers. *Biophys. J.* **2007**, *92*, 3817−3829.
(61) Case, D.; Ben-Shalom, I.; Brozell, S.; Cerutti, D.; Cheatham, T., III; Darden, T.; Duke, R.; Ghoreishi, D.; Gilson, M.; et al. *AMBER*; University of California: San Francisco, 2018.
(62) Jorgensen, W. L.; Chandrasekhar, J.; Madura, J. D.; Impey, R. W.; Klein, M. L. Comparison of simple potential functions for simulating liquid water. *J. Chem. Phys.* **1983**, *79*, 926−935.
(63) Machireddy, B.; Kalra, G.; Jonnalagadda, S.; Ramanujachary, K.; Wu, C. Probing the binding pathway of BRACO19 to a parallel-stranded human telomeric G-quadruplex using molecular dynamics binding simulation with AMBER DNA OL15 and ligand GAFF2 force fields. *J. Chem. Inf. Model.* **2017**, *57*, 2846−2864.
(64) Zhao, J.; Kennedy, S. D.; Turner, D. H. Nuclear Magnetic Resonance Spectra and AMBER OL3 and ROC-RNA Simulations of UCUCGU Reveal Force Field Strengths and Weaknesses for Single-Stranded RNA. *J. Chem. Theory Comput.* **2022**, *18*, 1241−1254.
(65) Cheatham, T. E. I.; Miller, J. L.; Fox, T.; Darden, T. A.; Kollman, P. A. Molecular dynamics simulations on solvated biomolecular systems: the particle mesh Ewald method leads to stable trajectories of DNA, RNA, and proteins. *J. Am. Chem. Soc.* **1995**, *117*, 4193−4194.
(66) Miyamoto, S.; Kollman, P. A. Settle: An analytical version of the SHAKE and RATTLE algorithm for rigid water models. *J. Comput Chem.* **1992**, *13*, 952−962.
(67) Roe, D. R.; Cheatham, T. E., III PTRAJ and CPPTRAJ: software for processing and analysis of molecular dynamics trajectory data. *J. Chem. Theory Comput.* **2013**, *9*, 3084−3095.
(68) Humphrey, W.; Dalke, A.; Schulten, K. VMD: visual molecular dynamics. *J. Mol. Graphics* **1996**, *14*, 33−38.
(69) Xu, L.; Sun, H.; Li, Y.; Wang, J.; Hou, T. Assessing the performance of MM/PBSA and MM/GBSA methods. 3. The impact of force fields and ligand charge models. *J. Phys. Chem. B* **2013**, *117*, 8408−8421.
(70) Golyshev, V. M.; Pyshnyi, D. V.; Lomzov, A. A. Calculation of Energy for RNA/RNA and DNA/RNA Duplex Formation by Molecular Dynamics Simulation. *Mol. Biol.* **2021**, *55*, 927−940.
(71) Braasch, D. A.; Corey, D. R. Locked nucleic acid (LNA): fine-tuning the recognition of DNA and RNA. *Chem. Biol.* **2001**, *8*, 1−7.

https://doi.org/10.1021/acsomega.2c07860
ACS Omega 2023, 8, 22382−22405

(72) Hanessian, S.; Schroeder, B. R.; Giacometti, R. D.; Merner, B. L.; Østergaard, M.; Swayze, E. E.; Seth, P. P. Structure-Based Design of a Highly Constrained Nucleic Acid Analogue: Improved Duplex Stabilization by Restricting Sugar Pucker and Torsion Angle γ. *Angew. Chem.* **2012**, *124*, 11404−11407.
(73) Levitt, M.; Warshel, A. Extreme conformational flexibility of the furanose ring in DNA and RNA. *J. Am. Chem. Soc.* **1978**, *100*, 2607−2613.
(74) Heinemann, U.; Roske, Y. Symmetry in nucleic-acid double helices. *Symmetry* **2020**, *12*, No. 737.
(75) Ho, P. S.; Carter, M. DNA Structure: Alphabet Soup for the Cellular Soul. In *DNA Replication-Current Advances*; IntechOpen, 2011.
(76) Xia, Z.; Bell, D. R.; Shi, Y.; Ren, P. RNA 3D structure prediction by using a coarse-grained model and experimental data. *J. Phys. Chem. B* **2013**, *117*, 3135−3144.
(77) Šponer, J.; Zgarbová, M.; Jurecka, P.; Riley, K. E.; Sponer, J. E.; Hobza, P. Reference quantum chemical calculations on RNA base pairs directly involving the 2′-OH group of ribose. *J. Chem. Theory Comput.* **2009**, *5*, 1166−1179.
(78) Butcher, S. E.; Pyle, A. M. The molecular interactions that stabilize RNA tertiary structure: RNA motifs, patterns, and networks. *Acc. Chem. Res.* **2011**, *44*, 1302−1311.
(79) Yakovchuk, P.; Protozanova, E.; Frank-Kamenetskii, M. D. Base-stacking and base-pairing contributions into thermal stability of the DNA double helix. *Nucleic Acids Res.* **2006**, *34*, 564−574.
(80) Parker, T. M.; Hohenstein, E. G.; Parrish, R. M.; Hud, N. V.; Sherrill, C. D. Quantum-mechanical analysis of the energetic contributions to π stacking in nucleic acids versus rise, twist, and slide. *J. Am. Chem. Soc.* **2013**, *135*, 1306−1316.

https://doi.org/10.1021/acsomega.2c07860
ACS Omega 2023, 8, 22382−22405